NOVA SCHOOL OF SCIENCE & TECHNOLOGY

DEPARTAMENT OF CHEMISTRY

SARA RODRIGUES AMORIM

BSc degree in Chemical and Biochemical Engineering

WATER ENHANCEMENT ON CO_2 ADSORPTION:

EQUILIBRIUM STUDIES ON AN AMINE SORBENT FOR DIRECT AIR CAPTURE

MASTER IN CHEMICAL AND BIOCHEMICAL ENGINEERING

NOVA University Lisbon

September, 2022

NOVA SCHOOL OF
SCIENCE & TECHNOLOGY

DEPARTAMENT OF CHEMISTRY

WATER ENHANCEMENT ON CO_2 ADSORPTION:

EQUILIBRIUM STUDIES ON AN AMINE SORBENT FOR DIRECT AIR CAPTURE

SARA RODRIGUES AMORIM

BSc degree in Chemical and Biochemical Engineering

Adviser: D. F. Wim Brilman
Full Professor, University of Twente

Co-advisers: H. Michel Schellevis,
PhD Candidate, University of Twente

Examination Committee:

Chair: Professor Doctor Teresa Maria Alves Casimiro Ribeiro
Assistant Professor, FCT-NOVA

Rapporteur: Doctor Rui Pedro Pinto Lopes Ribeiro
Researcher, FCT-NOVA

Members: Professor Doctor Mário Fernando José Eusébio
Assistant Professor, FCT-NOVA

MASTER IN CHEMICAL AND BIOCHEMICAL ENGINEERING

NOVA University Lisbon
September, 2022

Water Enhancement on CO_2 Adsorption: Equilibrium Studies on an Amine Sorbent for Direct Air Capture.

Dedico este trabalho aos meus pais,
amigos e ao meu parceiro.
O caminho é longo, mas vocês tornam-no menos difícil.

I dedicate this work to both my parents,
friends, and partner.
The road is long, but you make it easier.

ACKNOWLEDGMENTS

This work would not exist without the contribution of some people, for which I would like to express my gratitude. First, I want to thank my supervisors for the opportunity to partake in such an innovative assignment.

To Professor Wim Brilman, for accepting me in this research group, making sure that I had all the settings. For the kindness.

To Michel Schellevis, for having accompanied me in all the tasks and for being one of the professionals who contributed the most to my learning and training during this final phase of my academic career. Words cannot describe my gratitude for all availability to arrange meetings with me, whether in person or online, for the friendliness and excellent capacity for delegation.

To Professor Mário Eusébio who was always accessible to help me and answer to every question, an e-mail or videocall away.

To the SPT Group and University of Twente, where I was warmly welcomed. I would also like to thank the NOVA University of Lisbon for the working conditions it has provided over the years, enabling me the conclusion of this master's degree.

To my parents, brother and family who have always supported me and ensured the best conditions to achieve the goals I set for myself. Finally, to my friends and partner whose support and inspiration is crucial to becoming the best version of me. All my achievements are yours too!

To all, thank you very much!

"Success is not final; failure is not fatal:
It is the courage to continue that counts."
Winston S. Churchill

ABSTRACT

This work aims to establish a relationship between CO_2 adsorption capacity and water, in the context of CO_2 removal directly from atmosphere (DAC). For this, experimental data was obtained for a broad range of humidity, temperatures and concentrations of CO_2, using a supported amine sorbent. Subsequently, the CO_2 adsorption results were fitted to equilibrium models from literature and compared with experimental trends. The Stampi-Bombelli and WADST models revealed the best fittings, being both values of SSR and R^2 relatively close (SSR=0.338, R^2=0.969 and SSR=0.360, R^2=0.968, respectively).

The measurements were performed through the breakthrough method, on a pilot scale setup. These were featured with previous experimental work from SPT group for the same subject. After comparing both data sets, it was observed that the adsorbent had suffered ~20% degradation. Consequently, a correction factor was applied into previous values.

Experimental results displayed some inconsistencies, which were attributed to the uncertainty of the correction factor and the complexity of co-adsorption mechanisms. The maximum observed amount of CO_2 adsorbed/kg of adsorbent was 2.25 kg.mol^{-1} (P_{CO2}=1000 Pa, T= 5ºC, RH= 84.97%), and ~2.7 mol.kg^{-1} after the correction factor, which is significantly close to values found in literature. The CO_2 capacity under the presence of water in comparison with dry conditions (q/q_{dry}) was also considered to account its enhancement. At P_{CO2}= 40 Pa, the capacity adsorption nearly doubled in presence of high moisture content, while at the higher partial pressures (P_{CO2}=1000 Pa), humidity seemed to have a reduced impact.

For DAC conditions, experimental trends were well characterized, which follows literature remarks. Overall, the WADST and Stampi-Bombelli model represented the closest fits. In addition, an empirical model was proposed based on the observation of experimental trends. The model is described by a linear function, in which both values of slope and y-intercept were obtained through logarithmic equations.

Keywords: CO_2 capture, water vapor, direct air capture, co-adsorption, amine sorbent

RESUMO

A tese visa estabelecer uma relação entre a capacidade de adsorção de CO_2 e água, no contexto de captura de CO_2 diretamente da atmosfera. Para tal, dados experimentais foram adquiridos dentro de um intervalo amplo de temperaturas, concentrações de CO_2 e água, usando um adsorvente de aminas. De seguida, os dados foram ajustados a modelos mecanísticos da literatura e comparados. Os modelos Stampi-Bombelli e WADST foram os que melhor descreveram tendências experimentais, apresentando ajustes próximos (SSR=0.338, R^2=0.969 e SSR=0.360, R^2=0.968, respetivamente).

As medições foram realizadas através do método *breakthrough*, numa instalação piloto de laboratório. Os valores foram complementados um trabalho experimental previamente realizados no grupo SPT para o mesmo tópico. Após comparar os dados, observou-se que o adsorvente sofreu uma degradação de ~20%. Consequentemente, foi aplicado um fator corretivo a valores anteriores.

Os resultados experimentais mostraram algumas inconsistências, que por sua vez foram atribuídas à incerteza do fator de degradação e à complexidade dos mecanismos de co-adsorção. A quantidade máxima registada de CO_2 adsorvido/kg de adsorvente foi de 2.25 $kg.mol^{-1}$ (P_{CO2}=1000 Pa, T=5ºC, RH=84.97%), e ~2.7 $mol.kg^{-1}$ após a fator corretivo, que é significativamente próximo da literatura. A quantidade de CO_2 adsorvido em condições húmidas em relação à de condições secas (q/q_{dry}) também foi considerada para quantificar o seu acréscimo. Nas condições de P_{CO2}= 40 Pa, a capacidade de adsorção quase duplicou na presença de um alto teor de água, enquanto que a níveis superiores de pressão parcial (P_{CO2}=1000 Pa), foi observado um impacto reduzido na capacidade.

Para condições DAC, as tendências foram bem caracterizadas, paralelamente a observações da literatura. O modelo WADST e Stampi-Bombelli foram os que mais se aproximaram dos valores deste trabalho. Foi também proposto um modelo empírico com base em tendências experimentais. O modelo é descrito por uma função linear, cujos valores de declive e ordenada foram obtidos a partir de equações logarítmicas.

Palavras-chave: captura de CO_2, vapor de água, captura direta do ar, co-adsorção, adsorvente de aminas

CONTENTS

LIST OF FIGURES

LIST OF TABLES

Acronyms and Initialisms

APDES	Aminopropylmethyldiethoxysilane
BECCS	Bioenergy with Carbon Capture and Storage
BET	Brunauer–Emmett–Teller
CCS	Carbon Capture and Storage
CCU	Carbon Capture and Utilization
DAC	Direct Air Capture
DACCS	Direct Air Carbon Capture and Storage
DVB	Divinylbenzene
FTIR	Fourier transform Infrared
GAB	Guggenheim–Anderson–de Boer
GHGs	Greenhouse Gases
IPCC	Intergovernmental Panel on Climate Change
IR	Infrared
MEA	Monoethanolamine
MFC	Mass Flow Controllers
NETs	Negative Emissions Technologies
NMR	Nuclear magnetic resonance
PSA	Pressure Swing Adsorption
RH	Relative Humidity
SAS	Supported Amine Sorbents
SPT	Sustainable Process Technology
SSR	Sum of Squared Residuals

SST	Sum of Squares Total
TGA	Thermal Gravimetric Analysis
TSA	Temperature Swing Adsorption
WADST	Weighted-Average Dual-Site Tóth
WC	Working Capacity

SYMBOLS

$\boldsymbol{A}$	mol.kg^{-1}	Critical water loading
$\boldsymbol{b}$	Pa^{-1}	Equilibrium constant
$\boldsymbol{b_0}$	Pa^{-1}	Equilibrium constant at the reference temperature
$\boldsymbol{b_{wet}}$	Pa^{-1}	Equilibrium constant under wet conditions
$\boldsymbol{C}$	-	BET constant
$\boldsymbol{C_{G,0}}$	-	Entropic nature between the first and multilayer
$\boldsymbol{C_{ppm}}$	ppm	Concentration
$\Delta\boldsymbol{G}$	J	Gibbs free energy
$\Delta\boldsymbol{H}$	J.mol^{-1}	Enthalpy
$\boldsymbol{\Delta H_{ads}}$	J.mol^{-1}	Enthalpy of adsorption
$\Delta\boldsymbol{H_C}$	J.mol^{-1}	Enthalpy difference between monolayer and multilayer sorption
$\boldsymbol{\Delta H_{ave}}$	J.mol^{-1}	Average adsorption enthalpy
$\boldsymbol{\Delta H_{wet}}$	J.mol^{-1}	Adsorption enthalpy under humid conditions
$\boldsymbol{\Delta H_{vap}}$	J.mol^{-1}	Enthalpy of vaporization
$\Delta\boldsymbol{H_K}$	J.mol^{-1}	Difference between heat of water condensation and the heat of sorption of a multimolecular layer
$\Delta\boldsymbol{S}$	J.mol^{-1}	Entropy
$\boldsymbol{f_{blocked}}$	-	Fraction of blocked sites by hydrogen-bonded water structures
$\boldsymbol{f_{blocked,max}}$	-	Maximum fraction of blocked sites
$\boldsymbol{F_v}$	m^3.s^{-1}	Flow rate
$\boldsymbol{k}$	-	Fit parameter
$\boldsymbol{K_0}$	-	Entropic nature between the bulk liquid and the multilayer
$\boldsymbol{K_{ads}}$	-	GAB correction factor
$\boldsymbol{m}$	kg	Mass
$\boldsymbol{M_{gas}}$	g.mol^{-1}	Gas molar mass
$\boldsymbol{n}$	-	Fit parameter

P	Pa	Total Pressure
p	Pa	Partial Pressure
P^{sat}	Pa	Saturation Pressure
P^{W}	Pa	Partial vapor pressure
q	mol.kg^{-1}	Adsorption capacity
q_m	mol.kg^{-1}	Monolayer adsorption capacity
q_s	mol.kg^{-1}	Maximum adsorption capacity
q_{s0}	mol.kg^{-1}	Maximum adsorption capacity at the reference temperature
$q_{s,wet}$	mol.kg^{-1}	Maximum adsorption capacity under humid conditions
R	m^3·Pa·K^{-1}·mol^{-1}	Ideal gas constant
R^2	-	Coefficient of determination
T	°C	Temperature
T_0	°C	Reference temperature
t	-	Surface heterogeneity factor
t_0	-	Surface heterogeneity factor at the reference temperature
t_{wet}	-	Surface heterogeneity factor under humid conditions
X^{W}	-	Mole fraction of water
$\hat{y}_i$	-	Predicted value
$\bar{y}$	-	Mean of observations
α	-	Fit parameter
β	-	Co-adsorption parameter
ϕ	-	Amine efficiency
ϕ_{dry}	-	Amine efficiency under dry conditions
$\phi_{available}$	-	Fraction of available amine sites
ϕ_{max}	-	Maximum amine sites
γ	-	Co-adsorption parameter
χ	-	Fit parameter
∅	m^3.s^{-1}	Volume flow

1

INTRODUCTION

1.1 Problem Background

Global warming, described as a largescale increase of global temperatures, has led to environmental issues such as melting of snow cover and ice caps, rising sea levels, and more severe weather patterns [1]. Cook *et al.* [2] gathered a synthesis of published peer-reviewed journals showing that 97% or more of the scientific community agree that climate-warming trends over the past century are extremely likely due to human activities. The growth of world population and overall industry causes increasing emissions of greenhouse gases (GHGs), a group of gaseous compounds capable of absorbing and emitting radiant energy within the thermal infrared range [3]. This category includes, among others, water vapor, carbon dioxide, methane, nitrous oxide, ozone and various fluorinated gases. Among these, CO_2 is by far the most abundant human-caused greenhouse gas, and persists in the atmosphere and oceans for thousands of years after it is emitted [4].

The Paris Agreement has set a goal to limit global warming to "well below 2 ºC", preferably to 1.5 ºC, compared to pre-Industrial levels [5]. Figure 1.1 represents temperature data showing fast warming in the past few decades, the latest data going up to 2021 [6]. Alongside this illustration, a similar growing trend represents CO_2 concentrations in the atmosphere, steadily increasing every year (Figure 1.2). Here, the levels increased from 280 ppm, before the Industrial Revolution, to an average of 419 ppm in 2021. This is the highest level since accurate measurements began 63 years ago, according to NOAA and Scripps Institution of Oceanography [4]. Following the 2021 report of the Intergovernmental Panel on Climate Change (IPCC) [7], there is more than a 50% chance that the 1.5 ºC goal is crossed between 2021 – 2040 (with a central estimate of the early 2030s). Under a high-emissions scenario, the world reaches the 1.5 ºC threshold even more rapidly (2022 – 2037). Despite these predictions, the same report states that it is still within reach limiting global warming to 1.5 ºC by the end of the century, requiring advanced technologic transitions.

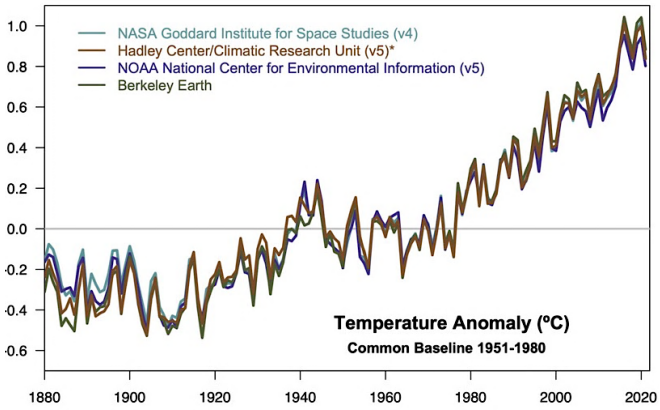

Figure 1.1 - Temperature data showing rapid warming in the past few decades, the latest data going up to 2021. According to NASA, 2016 and 2020 are tied for the warmest year since 1880, continuing a long-term trend of rising global temperatures [5].

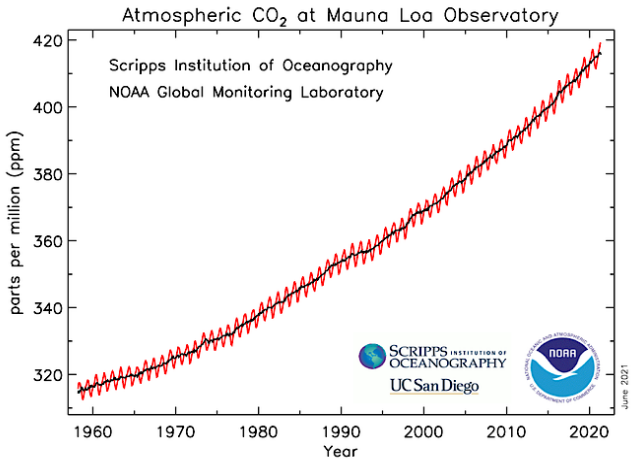

Figure 1.2 - Upward trajectory of carbon dioxide in the atmosphere. The annual fluctuation is known as the Keeling Curve. Image provided by NOAA Global Monitoring Laboratory, Boulder, Colorado, USA (https://esrl.noaa.gov/) [4].

Numerous solutions have been proposed to lower the CO_2 emissions of high-energy services such as aviation, long-distance transport and shipping, or for provision of energy. Ranging from carbon-free renewable resources to cleaner coals, or retrofitting power plants with the utilization of other types of fuel, such as natural gas [8]. It is unclear, however, whether these resources can be deployed rapidly and widely enough and overcome socio-political obstacles related to cost, environmental impacts, and public acceptance [9].

Alternatively, Carbon Capture and Storage (CCS) has been employed to at large point sources such as power plants, oil refineries, and in steel and cement production [10]. To offset GHGs emissions, most of the CO_2 produced by fossil fuels is captured locally and subsequently stored in underground reservoirs. In situ CCS can be divided into three categories, depending on where and how CO_2 capture is implemented: (1) pre-combustion capture; (2) post-combustion capture; and (3) oxy-fuel combustion. Among these processes, post-combustion stands out as the most economically viable option [8], [11]. It is possible to design carbon

capture in existing power plants with post-combustion capture, unlike the previous two, without compromising the existing operation and thus, providing a faster transition [10]. It requires less total investment and indirect costs, including utilities [8]. Moreover, it is considered a safe option due to its mature technology, whose first techniques (i.e. scrubbing the gas stream with a chemical solvent) were established over 60 years ago [8], [10].

Today, the most developed capture process is CO_2 absorption by aqueous alkanolamine solutions, typically monoethanolamine (MEA), where CO_2 is selectively absorbed by the reactive solvent in a scrubber. The CO_2-rich amine solvent is then sent to a stripper, where it is heated, and the CO_2 is released from the solution and compressed for transport and sequestration [12]. The main disadvantage, however, stands in the reduced CO_2 concentration present in the flue gas (i.e. 12 – 14 vol% for coal-fired and around 4 vol% natural-gas-fired), causing an increase associated to the total costs of the operation [13].

As for storage, the only potential storage sites with capacity for such quantities (Gt of CO_2 per year) are natural reservoirs, such as geological formations or the deep ocean. An alternative is injection of CO_2 underground, similar technology to the enhanced oil recovery employed by the oil and gas industry, and to the underground injection of waste as practiced in the USA [10]. This approach might be debatable since in some cases it could lead to an increased production of hydrocarbons, worsening the energy dependency on fossil fuels. Another drawback is storage space which, even though abundant, is limited and has associated costs of compression, transportation and pumping. Another option would be utilization of CO_2 (CCU) rather than storing it, which could alleviate the costs associated. Some of the applications of CO_2 range from turning it to other chemicals or fuels, solid inorganic carbonates, or for algae cultivation [10], [14].

Nevertheless, even if all the CO_2 product from flue gas is captured and permanently stored underground, the CCS process still falls short in achieving carbon neutrality [15]. In order to achieve the ambitious carbon reduction goals announced by the IPCC, point-source CCS requires complementary technologies [16]. Therefore, investigations for future management of climate change have involved the development on Negative Emissions Technologies (NETs), as a means of withdrawing GHGs from the atmosphere. NETs can be assigned into the following categories [5]:

1) Afforestation and reforestation;
2) Land management to increase and fix carbon in soils;
3) Bioenergy with Carbon Capture and Storage (BECCS);
4) Enhanced weathering;
5) Direct Air Capture of CO_2 with Carbon Capture and Storage (DACCS);
6) Ocean fertilization to increase CO_2.

These options include nature-based solutions (e.g., afforestation and restoration of marine habitats), measures to enhance naturally occurring processes (e.g., land management approaches to increase the carbon content in soil) and other technology-based solutions such as Bioenergy with Carbon Capture and Storage (BECCS). In the case of BECCS, atmospheric CO_2 is also removed by purpose-grown plants and trees, which are then converted to biomass. The

biomass can be burned to generate heat and electricity or turned into liquid fuels (known as biofuels), with the majority of CO_2 released during combustion being captured, liquefied, and stored [17]. Both afforestation and BECCS, however, involve high requirements of land availability of fertile soil, water and fertilizers, which may trigger potentially adverse concerns for food security and biodiversity [18]. Recent assessments have considered Direct Air Carbon Capture and Sequestration (DACCS) as a favorable technology that can potentially remove higher amounts of CO_2 than other NETs [14].

1.2 Direct Air Capture (DAC)

The concept of capturing CO_2 from air was first introduced for climate change mitigation by Lackner *et al.* in 1999 [19], and it serves as a promising addition to point-source capture by addressing emissions from distributed sources, which would otherwise be inaccessible to conventional CCS plants [16]. Additionally, its feed is air - it is everywhere and contains very low to null concentrations of contaminants that are present in flue gases, such as NO_x and SO_x. Thus, the equipment can be set in any location without concerning about the adsorbent poisoning [15] nor competing with agricultural and residential land uses [13].

On the other hand, DACCS still has some clear disadvantages compared to CO_2 capture from large point sources, which could prove challenging when deploying the technology at major scales. The fundamental issue is directly associated with the low concentration of atmospheric CO_2, 400 ppm, a factor of 100 – 300 times more dilute than the CO_2 concentration in gas- and coal-fired power plants [14]. This causes a massive disproportion between treated air flowrate and the mass of captured CO_2, e.g., for a CO_2 concentration of 400 ppm, at least 1400 m^3 of air needs to be supplied to capture 1 kg of CO_2 [13], considering the unlikely event of every CO_2 molecule is captured. In order to obtain a significant amount of CO_2, DAC plants need to operate with large volumes of air. Thus, DAC is more energy intensive than other CO_2 capture methods. Techno-economic reports on this matter estimate that the price of a DAC operation evolves somewhere 94 – 600 $/tCO2, depending on the technology, as opposed to 80 $/t$CO_2$ for CCS from a coal power station [20]. Despite the costs, the relative immaturity of DACCS technology indicates that there is considerable scope for innovation and cost reduction [18]. Moreover, in 2021 there were already 19 direct air capture (DAC) plants operating worldwide [21]. Table 1.1 holds public information about the three most advanced and industrialized companies on capturing carbon from the atmosphere.

Table 1.1 - Public information on the main commercial DAC entities, based on the data gathered by McQueen et al. [22].

	Carbon Engineering [23], [24]	**Climeworks** [13], [18], [21]	**Global Thermostat** [25], [26]
Founding year	2009	2009	2010
Location	Canada	Switzerland and Iceland	United States
Technology	Liquid Absorption	Solid Adsorption	Solid Adsorption
Capacity (t_{CO2} yr^{-1})	~ 365	~ 1000	~ 1000
Required temperature for energy needs (°C)	900	80 – 120	85 – 100
Thermal energy source	Natural gas with CCS.	Non-fossil energy resources (geothermal, waste heat, etc.)	– [1]
Current Costs ($. tCO_2^{-1})	– [1]	500 – 600	– [1]
Projected Costs ($. t_{CO2}^{-1})	94 – 232 [2]	200 – 300 within 5 years.	– [1]
Developments	Building the first large-scale DAC plant with a capacity of 1 $MtCO_2$ $year^{-1}$ by 2024.	First commercial DAC plant capturing 900 tCO_2 yr^{-1} delivered to a next-door greenhouse (2015).	Pilot plant in Melano Park, CA. Planning on building two pilot scale plants with the capacity of 3000–4000 tCO_2 yr^{-1}.

Two technologies are currently being used to capture CO_2 from the air: liquid and solid DAC. Liquid systems place ambient air into contact with a strong liquid base, such as potassium hydroxide (KOH) or sodium hydroxide (NaOH), which dissolves the CO_2 into a carbonate solution. CO_2 is then removed in a precipitator through the regeneration of the base, forming solid calcium carbonate ($CaCO_3$). Subsequently, the precipitate is sent to a calciner, where it reacts at extremely high temperatures (about 800ºC) with oxygen from an air-separation unit, forming calcium oxide (CaO) and pure CO_2, which can either be stored or used [18].

Solid DAC technology is based on supported amine sorbents (SAS) that adsorb (rather than absorb) atmospheric CO_2. These SAS consist of a porous support material with amine functional groups immobilized on or grafted to its surface, removing the need for H_2O and

[1] No data concerning this topic is publicly available.
[2] This range is reflected from a scenario by Keith *et al*. [23] The scenario represents a system optimized for air-to-fuels, where hydrogen is produced via electrolysis which results in an oxygen byproduct. The need for an air separation unit is removed as the oxygen is provided from electrolysis, additionally reducing electricity requirements.

thus being entitled as a "solid sorbent" [27]. When the sorbents are heated and/or placed under a vacuum, they release the captured CO_2, which is then collected for storage (CCS) or for use (CCU). Figure 1.3 illustrates the two-step process: step 1 consists of the adsorption of ambient CO_2, while step 2 presents the separation of the CO_2 using relatively low-temperature heat (around 100ºC or less), pressure or humidity changes, or some combination of these, to regenerate the sorbent [18].

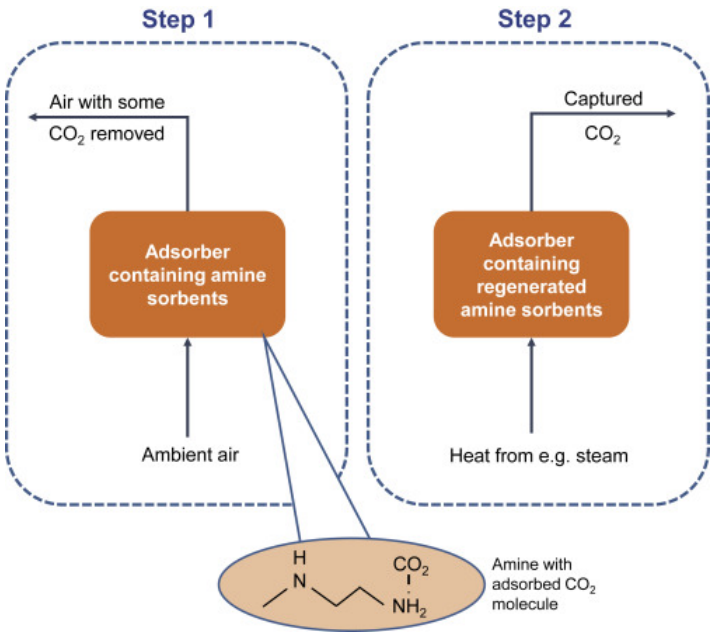

Figure 1.3 - Direct Air Capture using amine-functionalized solid sorbents based on Global Thermostat and ClimeWorks plant process descriptions [18]. Reproduced from Gambhir et al. (2019) under the Creative Commons license: http://creativecommons.org/licenses/by/4.0.

As opposed to the use of liquid solvents, SAS's appear as a cost-effective alternative [28]. According to previous evaluations of sorbent efficiency in CO_2 capture [29], solid sorbents represent a significant advantage due to the reduced corrosion, water- loss problems and mild regeneration conditions [15]. Furthermore, less energy is required to separate the CO_2 from the amine sorbent because adsorption results in a weaker bond between the CO_2 and sorbent when compared with absorption into a strong base [21].This work will focus on the application of a solid sorbent.

1.3 Problem Definition

The conditions in which CO_2 is captured from ambient air, referred to as "air capture", are considered humid. This is due to the significant concentrations of water in the air (10 – 50,000 ppm), as opposed to the very low CO_2 concentration of approximately 400 ppm [30]. Thus, the effect of water vapor requires consideration in any study related to carbon sequestration under

a DAC setting, whether for a real-world separation application or on a molecular scale. However, the studies on direct air capture are yet in an early stage. There are quite a few research gaps for the CO_2 - H_2O interaction in these conditions, which bring the motive to this thesis. The ones identified as the most relevant are as follows: (1) The relative humidity ranges that have been explored are either very narrow (one to two values) or at very high values, often resulting in pore condensation into a liquid-like state. The understanding of the behavior of co-adsorbed moisture and CO_2 still remains incomplete under low RH (%) and low CO_2 coverage conditions [31], especially since water concentrations fluctuate largely in air; (2) Most experimental reports focus on capacity enhancement by the presence of water, but very few authors attempt to describe which molecular mechanisms might lead to that phenomena; (3) A mechanistically consistent mathematical description of this enhancement does not yet exist [32]. To further improve process design and lower the costs, a detailed model on the interactivity between CO_2 and H_2O needs to be developed, while considering the weather conditions and choice of adsorbent.

1.4 Research Goals

The main goal of this research is the following:

Describe the influence of water on CO_2 adsorption, in supported amine sorbents, under DAC conditions.

In order to fulfill it, the following subgoal needs to be addressed:

- Establish a correlation between CO_2 equilibrium capacity and physical factors, i.e., temperature, relative humidity and CO_2 partial pressure.

For this, the first step is to obtain experimental adsorption data that covers a broad range of humidity, temperature and concentrations of CO_2. Compare how both parameters of temperature and partial pressure influence adsorption under dry and humid conditions.

Then, describe mathematically water's effect on CO_2 adsorption, in Lewatit® VP OC 1065, and find a good fit to original experimental co-adsorption data. For this, the experimental data will be used to apply models already developed from mechanistic understanding. Evaluate how each model fits the experimental results, interpret each fitted parameter to its physical meaning. In case none display an accurate fit, develop my own equilibrium adsorption model based on the study of experimental trends.

2

THEORY AND LITERATURE STUDY

2.1 Adsorption Phenomena

Adsorption occurs whenever one or more components from a liquid or gas phase, the adsorbate, adhere to the surface of a solid, known as adsorbent [33]. This phenomenon differs from absorption, in which the species are dissolved into a liquid or solid. Absorption takes up the whole volume of the material, while adsorption is a surface phenomenon [34]. The interfacial layer involves the surface layer of the adsorbent and the adsorption space in which enrichment of the adsorptive can occur [35]. The transport phenomena of a gas molecule on the inner surface of porous solid sorbents can be differentiated into three stages [36], as follows:

1) **External Mass Transfer:** transportation of adsorbate molecules from the bulk through the film layer resistance to the interface;
2) **Internal Mass Transfer:** the molecules travel along the length of the pores, limited either by molecular or Knudsen diffusion. In the case of an absolute pressure difference inside the pores, viscous flow can play a role;
3) **Interaction/reaction:** the adsorbate reacts/interacts with the functional groups on the surface.

Considering the complexity of applying these concepts to monolayer and multilayer sorption, some authors [33] consider adsorption simply as pore filling. The reverse mechanism is classified as desorption. The desorption takes place as a regeneration step to fully remove the adsorbate so that a new cycle of adsorption can restart. Due to the exothermic nature of adsorption, the reverse mechanism can be induced by increasing the temperature, a temperature swing adsorption (TSA), or reducing the pressure, known as pressure swing adsorption (PSA).

Interactions between the adsorbate and adsorbent can be characterized as physical or chemical, based on the nature of the surface's forces. Physical adsorption involves Van der Waals forces, forming a weaker bound due to induced dipole-dipole interactions [33]. On the other hand, in chemical adsorption, molecules are firmly bound to the surface through a covalent bound and are subject to chemical reactions. Bonding energies in adsorption range from

about 5-40 kJ.mol^{-1} for physisorption, lower than energies of 40–800 kJ.mol^{-1} present in chemisorption [37]. Thus, the sorbent regeneration in chemical adsorption is found to be more energy-intensive and frequently cannot occur without changing the adsorbent's properties [34]. Besides the nature of the interaction, the affinity of a component towards a specific adsorbent depends on molecular characteristics such as size, shape, polarity, the system's partial pressure, and temperature.

2.1.1 Thermodynamics

Adsorption involves an attractive interaction between adsorbate molecules and the adsorbent, resulting in a superior release of energy when forming bonds than breaking them. Thus, its enthalpy value, ΔH_0, is negative, and the reaction is considered exothermic [38]. The molecules in the desorbed state have high configurational entropy, but when they are bound to the adsorbate's surface, the entropy is reduced, i.e., ΔS is also negative. Considering the Gibbs free energy equation presented below, its value (ΔG) is negative if the condition $\Delta H > T\Delta S$ is met, causing the adsorption to occur spontaneously. The phenomenon is described below (Equation 2.1).

$$\Delta G = \Delta H - T\Delta S \tag{2.1}$$

Once the reaction takes place, ΔH value decreases as adsorption continues, whereas $T\Delta S$ increases, and finally, ΔH becomes equal to $T\Delta S$ so that $\Delta G = 0$. In other words, the adsorption rate equals the desorption rate, and an equilibrium is reached. Rather than looking at the adsorption mechanism as a one-way reaction, ΔG_0 can change from positive to negative by manipulating the temperature. Therefore, equilibrium can shift towards adsorption by lowering the temperature or desorption with a significant temperature increase.

One of the most relevant properties for thermodynamic studies is the isosteric heat of adsorption, ΔH_{is} (kJ.mol^{-1}). It is defined as the heat of adsorption determined at constant loading, a specific combined property of an adsorbent–adsorbate combination.
The activation energy (kJ.mol^{-1}), Ea, is another significant standard as it determines the temperature dependency of the reaction rate. It is associated with chemisorption and can be defined as the energy barrier the adsorbate molecules must go through before they become strongly bonded to the surface [39]. According to the Arrhenius equation, the value can be determined from experimental measurements of the adsorption rate constant at different temperatures. In practice, the activation energy generally varies with surface coverage due to energetic heterogeneity and/or sorbate-sorbate interaction [33].

2.1.2 Equilibrium

The extent of the reaction is limited by equilibrium. Such behavior is usually described by the amount of sorbent loading q_e, as a function of partial pressure (gases) at a fixed temperature, denominated as an isotherm [38]. The isotherm is used to characterize and evaluate the most critical properties of an adsorbent, such as adsorbent affinity, capacity, adsorption mechanism, and quantitative distribution of adsorbate [40]. Several isotherm models have been developed, varying in complexity and applicability.

2.1.2.1 Tóth Isotherm

The Tóth isotherm has described CO_2 adsorption in Lewatit VP OC with good accuracy [27], [36]. The isotherm is an empirical extension to the Langmuir isotherm (see Appendix A.1), suitable in describing heterogeneous adsorption systems and valid for both low and high-end boundaries of the pressure range [41]. The lowest region is specifically relevant for studies based on DAC as they work around reduced concentrations of CO_2. The equations that make up the isotherm are represented between 2.2 and 2.5. The parameters q_s [mol.kg^{-1}], b [Pa^{-1}], and t [-] are temperature-dependent variables, and q_{s0} [mol.kg^{-1}], b_0 [Pa^{-1}], t_0 [-], α [-] and χ [-] require fitting.

$$q_e = \frac{q_s b P_{CO2}}{(1 + (bP_{CO2})^t)^{1/t}} \tag{2.2}$$

The parameters b and t in Equation 2.2 are specific for adsorbate-adsorbent pairs. If the value of t equals 1, the relative energies of the different adsorption sites are the same, and the Tóth isotherm becomes the Langmuir isotherm. Hence, the further its value deviates from unity, the more heterogeneous the system is. For this reason, t is considered to describe surface heterogeneity of the adsorbent and should not be = 1, otherwise the equation reduces to the Langmuir isotherm [41]. The variable b is an equilibrium parameter, defined as $b = \frac{k_{ads}}{k_{des}}$ [36].

$$q_s = q_{s0} \exp\left(\chi\left(1 - \frac{T}{T_0}\right)\right) \tag{2.3}$$

In equation 2.3, χ is a fit parameter that confers temperature dependence in the maximum equilibrium loading, q_{so}. Nevertheless, it has been assumed to be equal to 0 when considering the CO_2 adsorption behavior in Lewatit as chemical. In chemisorption, the number of available sites is determined by the number of functional groups on the adsorbent, independently of which temperature occurs [42].

$$b = b_0 \exp\left(\frac{\Delta H_{ads}}{RT_0}\left(\frac{T}{T_0} - 1\right)\right) \tag{2.4}$$

$$t = t_0 + \alpha \exp\left(1 - \frac{T_0}{T}\right) \tag{2.5}$$

Equation 2.4 causes the relationship between ΔH_{ads} and b_0 to be dependent on the arbitrary value of T_0, referred to as reference temperature. Further, in a proposed model for co-adsorption CO_2-H_2O, the equation is altered to remove this association [32]. Equation 2.5 includes both α, a fit parameter, and t_0, a surface inhomogeneity factor at the reference temperature.

2.1.2.2 GAB Isotherm

GAB serves as an extension of the BET isotherm to also account for capillary condensation. The BET isotherm is limited to a concentration range of 5 – 30% RH (see Appendix A.2). With the GAB isotherm this is extended to 85%. This model considers the sorption state of adsorbed molecules to be identical throughout the multilayer but different from that of the pure liquid [43]. Thus, a parameter K_{ads} [-] was included in the original BET equation.

The parameter K_{ads} is referred to as a "correction factor" since it adjusts the properties of the multilayer molecules relative to the bulk liquid, by accounting for the difference in free energy between these two states. The more the adsorbed molecules are structured in a multilayer, the lower the value for K_{ads}. When K_{ads} approaches 1, there is almost no distinction between multilayer and liquid molecules, reducing it to BET isotherm [44].

$$q_e = q_m \frac{C_G K_{ads} \frac{p_{H20}}{P_{H2O}^{sat}}}{\left(1 - K_{ads} \frac{p_{H20}}{P_{H2O}^{sat}}\right)\left(1 + (C_G - 1) K_{ads} \frac{p_{H20}}{P_{H2O}^{sat}}\right)} \tag{2.6}$$

$$C_G = C_{G,0} \exp\left(\frac{\Delta H_C}{RT}\right) \tag{2.7}$$

$$K_{ads} = K_0 \exp\left(\frac{\Delta H_K}{RT}\right) \tag{2.8}$$

The parameter ΔH_C [J.mol^{-1}] refers to the difference in enthalpy between monolayer and multilayer sorption. This value is expected to be positive, due to the exothermic interaction of water with primary sorption sites. The value of ΔH_k, instead, is equivalent to the difference between the heat of water condensation and the heat of sorption of a multimolecular layer. This value will be negative and smaller, since the multilayer molecules are less firmly bound.

The factors $C_{g,0}$ [-] and K_0 [-] deal with entropic nature between the first and multilayer, and between the bulk liquid and the multilayer, respectively. $C_{g,0}$ is expected to be smaller than 1, since the molecules prefer to be in the multilayer above the monolayer from an entropic point of view. Similarly, K_0 will be larger than 1, due to the high entropy of the molecules in the bulk liquid [44]. The saturation vapor pressure is temperature-dependent and can be described by the Antoine equation 2.9. The parameters A [-], B [-], and C [-] correspond to the Antoine constants.

$$\log\left(p_{H_2O}^{sat}\right) = A - \frac{B}{T - C} \tag{2.9}$$

2.2 Supported Amine Sorbents

The adsorbent constitutes a significant weight in designing a successful CO_2 capture operation. Some criteria must be considered when selecting the sorbent among the existing ones or when to develop a synthetically new one. An ideal sorbent would gather important parameters like adsorption capacity, capital cost, and multicycle stability. The absolute value of adsorption capacity tends to be one of the most focused metrics in research. However, it does not consider the renewability conditions. Thus, the working capacity (WC) is considered an equally important parameter, defined as the difference between capacity before and after the adsorption step, quantifying how much sorbent needs to be heated in the desorption to capture the same amount of CO_2 [29]. The higher the WC, the lower the sensible heat energy penalty of the process, and the respective capital cost can be reduced [27].

Thermal energy requirements take up most of the costs around separation [45]. The heat of adsorption is a crucial adsorbent characteristic to determine the extent of thermal effects. It measures the heat generated during the adsorption process and the heat required to complete the desorption step. An additional factor is selectivity, which in this case, is described as the affinity of CO_2 over other components present in the air (such as H_2O and N_2) to achieve high product purity. This measure can determine the feasibility of the operation, as the further separations needed to separate the desired adsorbate from the other components takes up additional costs, which can be costly. Furthermore, stability is as essential since it defines the lifetime of the sorbent, i.e., the number of adsorption cycles. The higher this number of cycles, the more the stability can be affected due to multiple factors such as operating temperature and the presence of O_2, CO_2, and steam [46]. Realistically, no practical adsorbent gathers all these conditions. Therefore, each adsorbent's strengths and weaknesses must be considered in the context of a practical adsorption process for effective CO_2 separation [29].

Amine-containing sorbents have been formerly differed into three classes: (1) class 1 sorbents, based on physical interaction through impregnating amines into the pores of a support; (2) class 2, consisting of amine functional groups covalently bound to their internal surface; and (3) class 3 sorbents, where amine monomers have been polymerized in situ, resulting in polyamine structures tethered to the walls. These three classifications are illustrated in Figure 2.1. While more recently, a 4th class of sorbents has been proposed: aminosilane-grafted silica surface and an additional layer consisting of physically impregnated amino polymer clusters enclosed by a net of aminosilanes [47]. Class 1 sorbents typically have a higher capacity than Class 2 sorbents due to their higher amine content [48], though their adsorption kinetics are typically mass transfer limited [28]. While the adsorption loading of class 2 and 3 sorbents is not as competitive as the impregnated ones, the high stability during regeneration has proven to be an advantageous trait [28], [46]. Choi *et al.* [28] observed that supported-

amine adsorbents have relatively large CO_2 capacities at low CO_2 partial pressures compared to other adsorbent types, which make them feasible candidates for DAC operations.

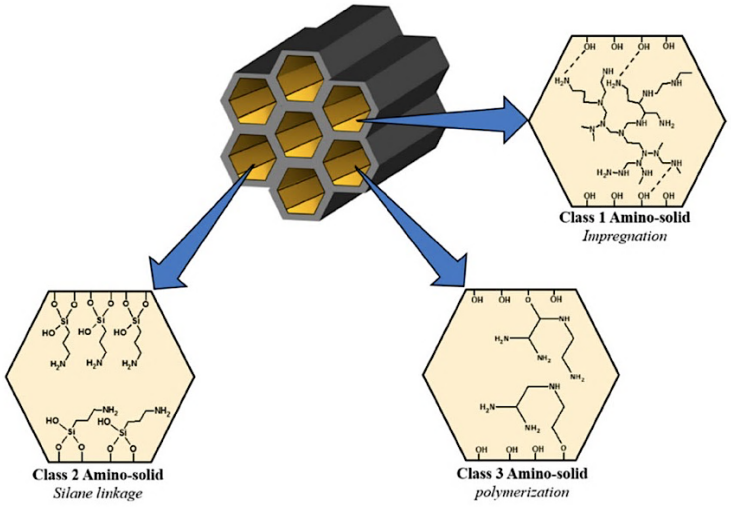

Figure 2.1 - Classification of amine sorbents [49], as previously defined by Didas [50]. Copyright © 2019, Springer Science Business Media, LLC, part of Springer Nature.

Among the research group Sustainable Process Technology (SPT), an analysis was performed to compare sorbents impregnated and grafted with amines [27]. By evaluating the adsorption capacity and thermal stability, impregnated amine sorbents were revealed to have a higher initial capacity due to their superior density of amines. However, these capacity values decrease substantially after a short period, as these amines are not attached to the surface they tend to evaporate during regeneration. On the other hand, grafted amine sorbents were shown to have much higher stability, despite scoring lower values in adsorption capacity. A grafted amine sorbent was found to be very stable and resistant to degradation and with a good capacity (q_{eq} = 3.2 mol.kg^{-1}), designated as Lewatit® VP OC 1065. The sorbent was the one chosen to be part of this study.

2.2.1 Lewatit VP OC 1065®

This study conducted experiments with the commercial mesoporous adsorbent Lewatit VP OC 1065®, imported from LANXESS [51]. The material is a polystyrene-based ion exchange resin (IER) containing primary benzylamine units (see Figure 2.2), with cross-linking for dimensional stability and a divinylbenzene (DVB) crosslinking. The resin comes in the form of spherically shaped beads [52], whose scanning electron microscope (SEM) capture is presented in Figure 2.3. The chemical and physical properties of this adsorbent are presented in Appendix B.1.

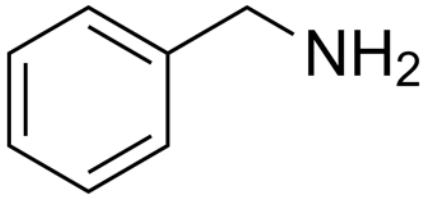

Figure 2.2 – Representation of a benzylamine structure.

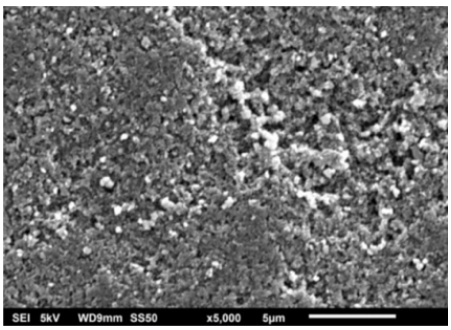

Figure 2.3 - A scanning electron microscope (SEM) capture of Lewatit VP OC 1065 beads [46].

While it was observed that the resin has similar capacities of CO_2 at ambient conditions when compared with other sorbents [13], Lewatit showed a high selectivity of CO_2 over H_2O (0.24 mol CO_2/ mol H_2O) in comparison to other alkali carbonate sorbents and physical sorbents under air capture conditions (P_{CO2} = 40 Pa, 20 °C, relative humidity (RH) = 58 %). Moreover, it is commercially available in large amounts, making it a good candidate for scaling-up. Alesi *et al*. [30] also reported that VP OC 1065 has a stable CO_2 capacity during 18 cycles and that can be almost entirely regenerated at temperatures in the order of 100 °C, a temperature that has lower risks of causing sorbent degradation.

In previous studies with Lewatit, it was experimentally observed a maximum capacity of 18.5 mol $H_2O.kg^{-1}$ (RH = 93%, T = 21.7ºC) [43] and 2.95 mol $CO_2.kg^{-1}$ (70 vol% of CO_2, T = 32.85ºC) [53]. As the maximum theoretical amine loading is expected to be in the order of 6.7 mol $N.kg^{-1}$ of sorbent [54], the maximum CO_2 loading then corresponds to a amine efficiency of 0.44 mol CO_2 per mol N_2.

Yu *et al.* [46] evaluated the thermal and chemical stability of Lewatit VP OC 1065 in view of the potential strategies of regenerating this sorbent in CO_2 removal application and reported significant oxidative degradation above 70°C in air and, surprisingly, above 120°C degradation in concentrated dry CO_2. In view of the degradation observed, sorbent regeneration should be carried out in absence of oxygen when operating above 70°C and at temperatures below 150 °C to avoid thermal degradation. If the partial pressure of CO_2 approaches 1 bar, the maximum temperature should not be higher than 120°C to avoid urea formation. Humidity was unable to completely prevent urea formation nor to reverse it.

The Tóth isotherm has described CO_2 adsorption in Lewatit VP OC with good accuracy [27], [36]. Figure 2.4 depicts the CO_2 behavior under dry conditions through the Tóth equilibrium model and fitted parameters determined by M. Bos et al. and Veneman et al. [27], [36],

based on experimental results. The CO_2 adsorption isotherms exhibits a typical Langmuir shape characteristic of chemisorption with a steep rise at low pressures and a plateau at higher pressures. Both sets of parameters have very similar trends, particularly in the lower partial pressure region. Furthermore, it displays comparatively high loadings of ~1 mol.kg^{-1} in ambient conditions, i.e., T = 25 ºC, P_{CO2} = 40 Pa, represented in Figure 2.4 a). While for the same conditions but at higher partial pressures, e.g., p_{CO2} = 1000 Pa, maximal loadings reach no more than 3 mol.kg^{-1}.

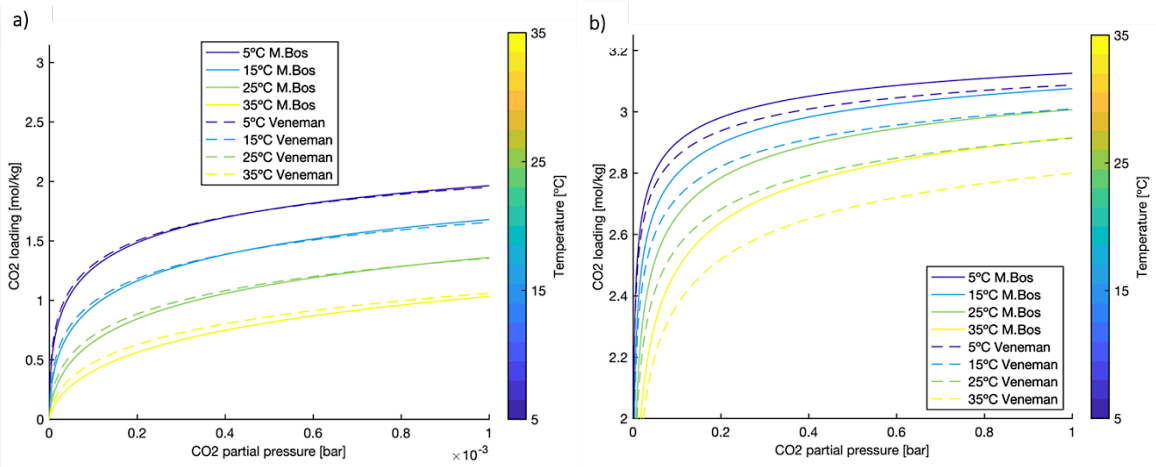

Figure 2.4 – CO_2 equilibrium isotherm for Lewatit VP OC for different temperatures [5-35 ºC] from two sets of parameters, M. Bos and Veneman [27], [36]. From left to right: a) sorbent loading within a lower partial pressure range [0-100 Pa]; b) overlook of the whole partial pressure array [0-1000 Pa]. The parameters are displayed in Appendix C.1.

Previous equilibrium experiments [53] have confirmed that water adsorption in Lewatit indeed behaves as physisorption. This assumption is based on (1) H_2O adsorption has displayed experimentally a much higher sorbent loading (q_e=12.5 mol.kg^{-1}) than CO_2 (q_e=2.5 mol.kg^{-1}) [52]; (2) the adsorption heat value for water is significantly lower than CO_2 ($\Delta H_{ads,H2O}$ = 43 kJ.mol^{-1}, $\Delta H_{ads,CO2}$ = 70−80 kJ.mol^{-1}), adding the fact that ΔH_{ads} is very close to the condensation heat of water ($\Delta H_{vap,H2O}$ = 41 kJ.mol^{-1}), suggesting that indeed condensation/pore filling occurs at higher relative humidity [53].

Figure 2.5 depicts the H_2O behavior applying the GAB equilibrium model and fitted parameters determined by J. G. Martínez [43], based on experimental studies. As opposed to CO_2, the kinetics for the adsorption of water vapor has not been studied in detail. Although it is known that physical adsorption processes are in general fast compared to chemical adsorption processes [27], which has been observed for the case of water [55].

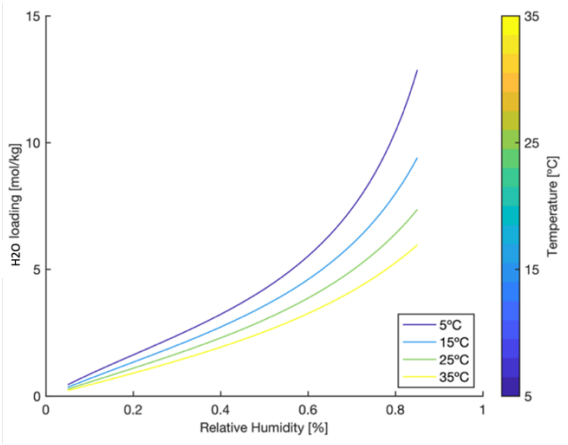

Figure 2.5 - Water equilibrium loading for Lewatit VP OC as a function of the relative humidity [5-85%] and temperature [5-35 ºC], using the GAB equilibrium model. The parameters applied are displayed in Appendix C.2.

2.3 Co-Adsorption Mechanisms

2.3.1 CO_2 Adsorption under Dry Conditions

The uptake of CO_2 in aqueous alkanolamines, which is the most intensively studied amine–CO_2 interaction, has most often been described as the formation of alkylammonium carbamates through a zwitterion mechanism for primary and secondary amines [28], [56]. For adsorption with amines supported, or tethered, on solids, the main mechanisms are still under investigation. Nonetheless, literature has consistently reported two species formed on amine-functionalized adsorbents in the presence of carbon dioxide, in anhydrous conditions: ammonium carbamate and carbamic acid. Such species were found in numerous spectroscopic studies based on Fourier transform infrared (FTIR) [31], [57]–[61], 13C solid-state NMR [62]–[64] and to a lesser extent, 15N NMR [64], [65] and X-ray diffraction [66]. In contrast, many described conflicting band assignments in FTIR studies and insensitivity in solid-state NMR (SSNMR), reason why the precise atomic-level structure of chemisorbed CO_2 species remains poorly understood [67].

The well-established mechanism between primary and secondary amines[3] and CO_2 was first proposed by Caplow *et al.* (1968) [37] and Danckwerts *et al.* (1979) [68] as an acid-base reaction. In the first step, amines act as a nucleophile (Lewis's base) adding to the carbonyl group of the CO_2 to form a zwitterion molecule, referred to as 1,3-zwitterion, where 1 and 3 indicate the positive and negative centers, respectively (equation 2.10). This nucleophilic "attack" involves the initial formation of a C–N bond to form carbamic acid in absence of adjacent amine groups, via intramolecular proton transfer, as illustrated in Figure 2.6 b) and equation 2.12.

[3] For the sake of context, while Lewatit VP OC contains merely primary amines, the literature approached in this chapter will only refer to primary and secondary amines, as they have similar mechanisms. Adsorption of tertiary amines, consequently, will not be discussed.

$$RNH_2 + CO_2 \rightleftarrows RNH_2^+COO^- \tag{2.10}$$

$$RNH_2^+COO^- + RNH_2 \rightleftarrows [RNHCOO^-][RNH_3^+] \tag{2.11}$$

$$RNH_2 + CO_2 \rightleftarrows RNHCOOH \tag{2.12}$$

The carbamic acid may be converted into a more stable carbamate salt via intermolecular proton transfer [69] if another amine is close enough or in the presence of pathways for proton migration, acting as a Brønsted base [52] (see Figure 2.6 a) and equation 2.11). The latter mechanism requires two amine groups per adsorbed CO_2 molecule (2:1 stoichiometry).

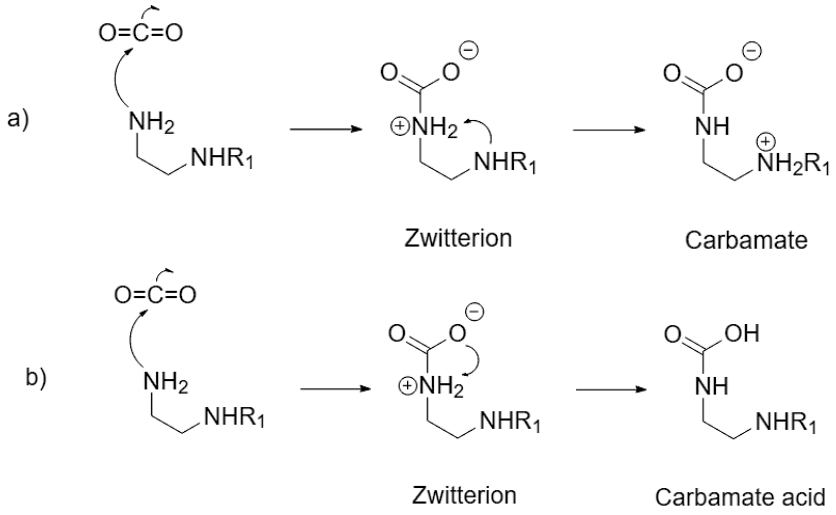

Figure 2.6 - CO_2 adsorption on primary/secondary amines via (a) the carbamate mechanism and by (b) the formation of carbamic acid. Based on the original publication of M. Hahn, M. Steib, A. Jentys, et al. [70]. Copyright © 2015, American Chemical Society.

Both the internal proton transfer to form the carbamic acid and the subsequent acid-base reaction to form the carbamate product would be expected to form fast. Therefore, the rate-determining step in the formation of ammonium carbamate is considered to be the nucleophilic addition of the amine nitrogen and CO_2 carbon [71]. This mechanism is applicable to sterically hindered amines as well, which are defined structurally as primary amines where the amino group is attached to a tertiary carbon atom, or secondary amines where the amino group is attached to a secondary or a tertiary carbon atom [28].

There is no experimental evidence of the existence of the zwitterion, not even in aqueous solutions [72]. A possible explanation is that the energetics of zwitterion formation are unfavorable, such that its concentration falls below the detection limit of spectroscopic techniques. As an alternative to the 1,3-zwitterion, other studies have pointed out that the nucleophilic attack of CO_2 could be assisted or catalyzed through hydrogen bonding by other species such as amine [73], water [30], or hydroxyl groups (OH) [72].

On a thermodynamic point of view, the energy barrier to the deprotonation step is high due to the transition state, which consists of a four-membered ring where the proton is intermediate between the amine nitrogen and the carbamate oxygen [72]. The second amine provides stabilization through hydrogen bonding, to both products and reaction intermediates, thus lowering the energy barriers [74]. Carbamic acids are not thermodynamically stable as they hydrogen bond to convert to ammonium carbamate, or dimerize, in form of paired carbamic acid (see Figure 2.7) [74]. An analysis of the C=O infrared frequency by Bacsik *et al.* [57] on silica modified by n-propylamine identified the presence of hydrogen-bonded carbamic acid and carbamate ions in dry conditions, which are formed rapidly. In a more recent study [64], it was suggested that both the ion pair ammonium carbamate and the neutral pair amine-carbamic acid are present in aminated silicas that have come into contact with CO_2.

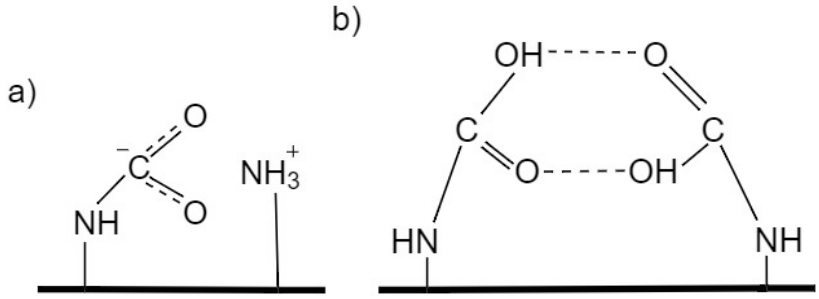

Figure 2.7 - Visual scheme of both species that CO2 adsorbs in the absence of water on amine-functionalized sorbents, being a) Ammonium carbamate and b) Paired carbamic acid. Based on the original publication of Young et al. [40].

According to Yu *et al.* [75], CO_2 adsorbs on primary amine as ammonium carbamate and secondary amine as carbamic acid. Another report [76] also observed this phenomenon based on situ infrared (IR) spectroscopy for different CO_2 capture conditions, including direct-air (0.04 vol%), where CO_2 adsorbs on the primary amine site as strongly adsorbed species in the form of ammonium carbamate, and the secondary amine site as weakly adsorbed species in the form of carbamic acid. However, the same study did not exclude the formation of different species on one amine-functionalized sorbent.

Moreover, reports have claimed that the resultant species are strongly influenced by (1) amine coverage (2) moisture and (3) amine steric hindrance [67]. Another article from Didas *et al.* [31], focused on the association between amine coverage and CO_2 mechanisms under dry and humid conditions. The authors used primary sorbents (APS) grafted to SBA-15 silica with three different levels of amine density. It appeared that "SBA-APS-low" formed ammonium carbamate ion pairs, hydrogen-bound carbamic acid and bound carbamate under dry CO_2 conditions, while "SBA-APS-high" only forms ammonium carbamate pairs in both dry and humid conditions. Others [57], [58], [67] observed similar results, i.e., more ion pairs formed on samples with high amine densities (silica/APMES) as opposed to those with low coverage (silica/APMDES).

When focusing on the sorbent of this study, Lewatit VP OC 1065, it is expected for its primary benzyl amines to interact with CO_2 to form either carbamic acid or a carbamate ion

[54]. Alesi *et al.* [54] mentioned that it is not possible to determine if the dominant captured species are carbamic acid or carbamate ion form. While more recently, a molecular modeling [30] on the same material showed that the amine groups could react with each other despite being fixated on the surface. It also pointed out that, under dry conditions, the most likely reaction mechanism corresponds to formation of carbamic acid, with an H-bridge to the remaining second amine. In this case, as there is neither a solvent (H_2O) nor a strong electrostatic field present, the authors stated that no stable ammonium carbamate could be established.

Theoretically, the formation of carbamic acid can indeed increase amine efficiency in CO_2 adsorption due to its stoichiometry of 1 mol of CO_2 to 1 mol of amine [32]. However, carbamic acid is said to be unstable, as mentioned before, without converting to carbamate or in its paired form. In addition, Didas *et al.* [73] observed that the activation barrier for the formation of carbamic acid using two amine molecules per CO_2 (ca. 16 kcal.mol^{-1}) was much lower than the for the one-to-one reaction (ca. 40−50 kcal.mol^{-1}). The intense reduction suggests that an additional amine molecule might be required to catalyze the reaction, giving it a stoichiometry of 2:1.

2.3.2 Water Adsorption

Understanding water adsorption performance is as relevant for this study as CO_2 since there is no way to avoid moisture in direct air conditions. A good understanding of some physical mechanisms is required, including the monolayer and multilayer formation, as well as capillary condensation.

Water behaves differently than CO_2, namely, by physisorption. In the first layer of water, all the adsorbed molecules are in contact with the surface, while subsequent layers have less interaction with the sorbent. As relative pressure rises, the thickness of adsorbed layers gradually increases, and multilayer adsorption occurs (layers 2–9). The molecules of the multilayers display energy levels somewhere between those of the monolayer and the liquid state [44]. Therefore, the energy of adsorption of the second layer is similar to the latent heat of vaporization of the adsorbate [77]. When relative pressure reaches initial capillary condensation pressure, water starts condensing inside the pores until they are filled [35], [43].

Once desorption takes place, hysteresis is observed as it is typically associated with capillary condensation. The phenomenon shows a different, higher curvature in equilibrium capacity when compared with adsorption. This is due to the altered angle of the adsorbate evaporation from the liquid meniscus. Figure 2.8 was picked as a representation of this phenomena, resultant from water adsorption experiments performed with Lewatit at T=8 ºC alongside a wide range of humidity (RH= 7–93%) [43].

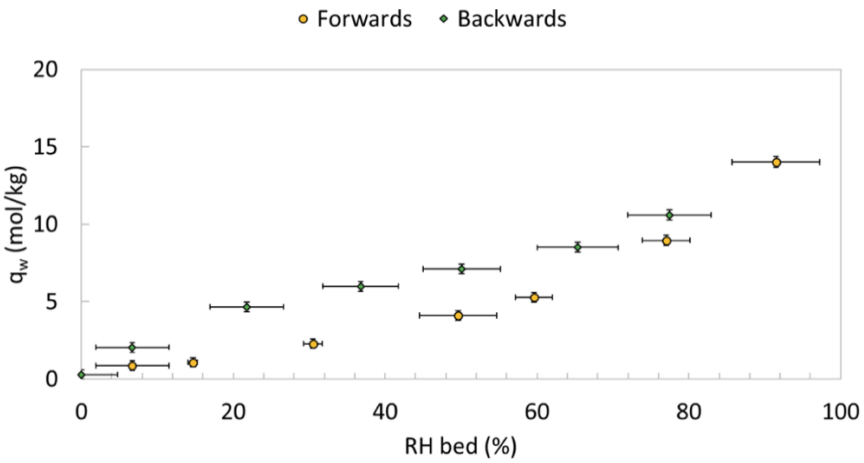

Figure 2.8 - Hysteresis behavior in Lewatit at T= 8ºC, shown by the adsorption equilibrium capacity of water as a function of RH (%), forwards and backwards [28].

2.3.3 CO_2 Adsorption under Humid Conditions

The role of water in the CO_2 capture on solid amine sorbents has shown to be ambiguous over its mechanisms at a molecular level. How H_2O molecules control the amine efficiency of the sorbent and which are the dominant species, is still under debate [78], [79]. In particular, distinguishing moisture-induced CO_2 species (e.g., bicarbonate) from carbamic acid or carbamates is considered a challenging assignment, mainly because the signals attributed to carbamic acid and carbamate species tend to dominate the FTIR and NMR spectra [78].

Although it has been observed that H_2O adsorption is unaffected by the presence of ultra-diluted CO_2 [80], a significant number of reports have proven experimentally that water does improve CO_2 capture efficiency both in aqueous and solid amine sorbents. Studies regarding solid sorbents witnessed that this effect was especially pronounced for low CO_2 concentrations [80], [81]. The work by Gebald *et al.* [80] was one of them, whose binary CO_2-H_2O studies were conducted on 3-Aminopropylmethyldiethoxysilane (APDES), a primary amine sorbent. CO_2 capacities were calculated at P_{CO2}= 40 Pa under the presence of water, which resulted in an enhancement of 92% and 1191% for adsorption at 296 and 323 K, respectively. The latter enhancement is particularly elevated, going from q_{dry}= 0.11 mol.kg^{-1} to q_{humid}= 1.42 mol.kg^{-1}. On a higher CO_2 concentration range, however, humidity only slightly enhances CO_2 adsorption (e.g., at P_{CO2}= 100 kPa and T= 296 K, capacity went from q_{dry}= 2.26 mol.kg^{-1} to q_{humid}= 2.54 mol.kg^{-1} in presence of humidity). Indeed, the CO_2-H_2O interaction is quite promising for future DAC technology, but analysis on a particle scale needs to be developed in-depth.

On the other hand, reduction on CO_2 capacity was detected in the presence of water, as opposed to what is commonly described in literature. Liu *et al.* [82] reported a decrease from 2.765 to 2.579 mmol.g^{-1} under flue gas conditions (e.g. CO_2 concentrations of 10% at

atmospheric pressure), which was attributed to possible blockage of the pores by accumulation of excess H_2O, or additional mass transfer resistance.
For primary and secondary amines, in aqueous adsorption systems, two types of reaction might occur: between H_2O – CO_2 – Amine, and H_2O – Carbamate species – Amine.

$$CO_2 + H_2O + RNH_2 \rightleftarrows HCO_3^- + RNH_3^+ \tag{2.13}$$

In the first reaction (equation 2.13), water acts as a nucleophile in contact with CO_2 to form carbonic acid, which in turn reacts with an amine. Because amine solvent solutions have a much higher pH than neutral water, they act as a more favorable Brønsted base to enhance the formation alkylammonium bicarbonate/carbonate products [69], [74], [83]. Carbonate species have been reported as unlikely as conditions that favor its formation (pH > 11) are not present [30], [84].

$$RNHCOO^- + H_2O \rightleftarrows HCO_3^- + RNH_2 \tag{2.14}$$

The second reaction involves water molecules hydrolyzing the initially formed carbamate species, releasing a free amine to produce ammonium bicarbonate [72], as indicated in equation 2.14. It should be mentioned that for each ammonium bicarbonate, the amine/CO_2 ratio is 1:1, whereas for an ammonium carbonate, the amine/CO_2 ratio is 2:1 (only 0.5 mol of CO_2 captured per amine). Figure 2.9 shows the molecules of both ammonium bicarbonate and water stabilized carbamic acid, as possible species that CO_2 adsorbs in the presence of water on amine-functionalized sorbents.

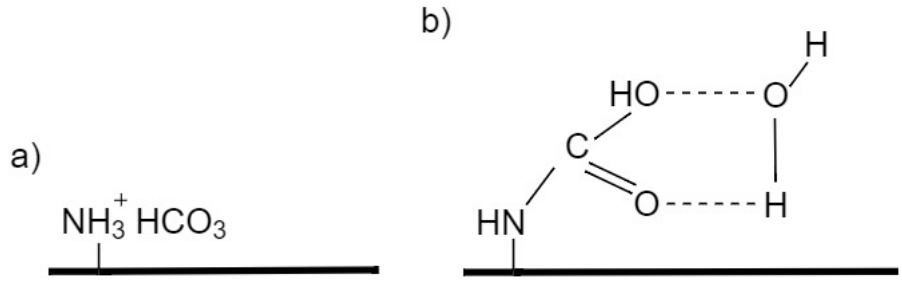

Figure 2.9 - Visual scheme of both species that CO_2 adsorbs in the presence of water on amine-functionalized sorbents, being a) Ammonium bicarbonate and b) Water stabilized carbamic acid. Based on the original publication of Young et al. [40].

The mechanisms that occur in aqueous systems may differ from the ones in grafted amines. Solid sorbents have its amine functional groups surrounded by neighboring amine and alkyl (C–H) groups instead of H_2O molecules. Furthermore, both environments differ in the number of H_2O molecules that interact with amine functional groups, adsorbed intermediates, and adsorbed CO_2 [79]. Indeed, ammonium bicarbonate, a specie actively present in aqueous amines, had not been unambiguously identified on grafted amine sorbents (primary and secondary) until a recent study by Didas *et al*. [31] under wet conditions. The same report that investigated the impact of amine coverage on adsorption detected the occurrence of bicarbonate on a grafted sorbent (e.g., SBA-APS low coverage), attributing it to the band formed

in the range of 1350 – 1360 cm^{-1} in the IR spectra. These findings support a zwitterionic mechanism transitioning slowly to bicarbonate in the presence of water, after rapid formation of ammonium carbamate. Additionally, the authors proposed a difference in humid adsorption behavior for supported amine adsorbents with varying degrees of amine loading, reinforcing the same proposition given in dry conditions: different adsorption mechanisms occur within different materials.

Although bicarbonate formation for this analysis was observed, other researchers did not report its presence under humid conditions, neither computationally nor experimentally (where the wet capacity would equal the double corresponding to the dry loading). The increase in amine efficiency has rather been justified by one (or more) of the following occurrences: (1) more carbamate ion pairs, as a result from water-induced proton transfer from carbamic acid to neighboring amines. [13], [57], [78], [85]; (2) formation water stabilized carbamic acid [30], [32]; (3) the release of additional hydrogen bonded amines [57].

In alternative to bicarbonate, Li *et al.* [72] found hydronium carbamate to form in larger concentrations than bicarbonate on a (PEI)-impregnated sorbent, based on a spectroscopic analysis. This phenomenon was justified by the weak energy of formation (−1 $kJ.mol^{-1}$) of bicarbonate when comparing to hydronium carbamate (−42 $kJ.mol^{-1}$). Hydronium carbamate was first proposed by Caplow for interpreting kinetics of carbamate formation and dissociation [37], [79], but very little information is presented on this mechanism. It has been proposed that a carbamate zwitterion stabilized by water is deprotonated, forming hydronium carbamate [15]. The reaction mechanism is as follows:

$$RNHCOO^- + H_2O \rightleftarrows H_3O^+ + RNCOO^- \tag{2.15}$$

The effect on adsorption is very similar for both hydronium carbamate and bicarbonate pathways, as each species only requires one amine group for CO_2 adsorption, as opposed to two for ammonium carbamate. Another mechanism suggested by Yu and Chuang [86] that carbamic acid can be interconverted to hydronium carbamate.

For experiments performed with Lewatit VP OC, the already referred molecular modelling by Buijs and de Flart [30] perceived that the most probable reaction corresponds to the formation of carbamic acid stabilized by water. The authors also claimed that water is directly involved in the proton transfer from amine – H_2O – amine – CO_2, i.e., the reaction is catalyzed by water. Quantum chemical calculations found the H_2O molecule to be located between the two benzyl amine groups, in contrast to previous studies [56], which could support the hypothesis of water not being just a polar spectator but actively participating in the proton transfer. The activation barriers under these conditions were found to be significantly lower (45 $kJ.mol^{-1}$) when compared to as the amine catalyzed case (76 $kJ.mol^{-1}$), i.e., dry conditions.

The same proposal for water stabilized carbamic acid as the main mechanism in humid conditions is supported by a more recent article by Young *et al.* [32], operating with the same sorbent. It was observed that co-adsorption enhancement in the lower pressure region would

be significantly superior, with values up to 2.5 times the adsorption capacity under dry conditions. The apparent disparity in adsorption enhancement within the partial pressure range led to the exclusion of ammonium bicarbonate or hydronium carbamate as possible species under humid conditions. As stated, "the high enhancement factors observed at low partial pressures would be expected to persist at higher partial pressures as each amine group that is used for adsorbing one CO_2 molecule under dry conditions can now adsorb two". Nonetheless, the study was not able to exclude the formation of other species (i.e., carbamate). The experiments were performed under three different temperatures (25 ºC, 50 ºC and 70 ºC), each at 0%, 30%, 55% and 80% relative humidity (RH). The breakthroughs were conducted at a CO_2 partial pressure range of 0,005 – 1 bar.

The work held by Yu *et al.* [13] did not detect either the presence of bicarbonate, given the absence of the HCO_3^- bond lays in the sorbent characterization. The peak observed was rather attributed to the $NCOO^-$ group, pointing towards carbamate formation, indicating that water co-adsorption does not alter the mechanism for dry CO_2 adsorption. Here, Lewatit was exposed to humid lab air (22 °C, 40 – 50% RH) for varying times, ranging from 17 min to 2.5 day. For the equilibrium experiments, illustrated in Figure 2.10, the water and CO_2 capacity were measured for wet air with a relative humidity (RH) of 10% – 80% at 15 – 40 °C. The representation of co-adsorption of H_2O results shows an increasing trend throughout relative humidity.

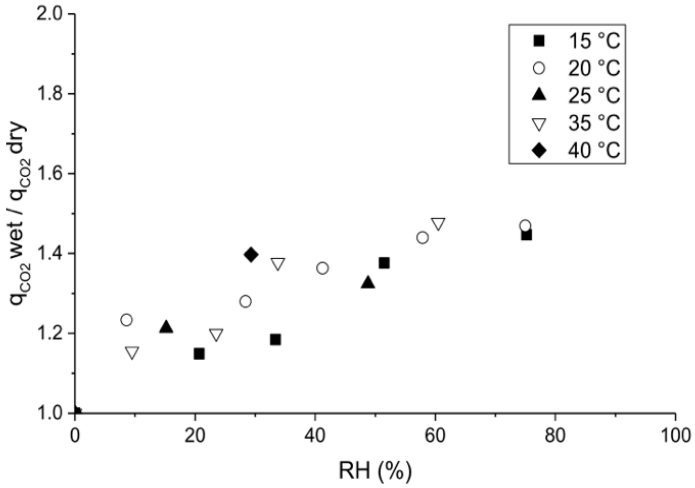

Figure 2.10 – Experimental results from Qiu et al. [13] performed with Lewatit VP OC. The ratio of CO_2 adsorption capacity at wet condition over dry condition as a function of RH (%) in the feed gas at five different temperatures (P_{CO2} = 40 Pa).

For the kinetics, the rate constant of CO_2 adsorption (K_{ads}) in humid air was found to be lower when compared with the one determined in dry air. This might be due to the water adsorption leading to an additional barrier for the mass transfer of CO_2 or for the heat evolved during the initial phase when the sorbent is loaded with water [13].

2.4 Co-Adsorption Models

The models presented below were considered in two studies dedicated to the co-adsorption analysis of CO_2 and water in solid amine sorbents [32], [45]. Both the Mechanistic co-adsorption model and the Weighted Average Dual Site Tóth (WADST) model were suggested by Young *et al.* [32], with the same sorbent as the one applied in this work, alongside the empirical co-adsorption model Stampi-Bombelli adapted from the work by Stampi *et al*. [45].

2.4.1 Tóth Transformed Equation

The equation used to describe the b parameter in the Tóth equilibrium model was re-arranged in the work of Young *et al.* [32], which is applicable to the Mechanistic and WADST Model. The original equation causes the relationship between ΔH_o [J.mol^{-1}] and b [Pa^{-1}] to be dependent on the arbitrarily assigned T_0 [°C]. For this reason, the authors changed the equation to remove this dependence. In order to have a consistent comparison of fits between Young *et al.* and this work's, the adjustment was applied.

$$b = b_0 \exp\left(\frac{-\Delta H_{ads}}{RT_0}\right) \tag{2.16}$$

2.4.2 Model Mechanistic

The following equilibrium isotherm is intended to approach three effects that were considered relevant in the CO_2-water adsorption behavior: (1) Amine efficiency may be limited by hydrogen-bonded water structures blocking CO_2 access to amine sites at high water loadings; (2) The presence of water can increase the stoichiometric ratio due to ammonium bicarbonate formation; (3) The presence of water changes the heats of adsorption of adsorbed CO_2 species hence the affinity. Based on these properties, the authors propose a mechanistic adjustment of isotherm behavior, as described in equations 2.17–2.21. First, a generic equation of CO_2 loading including terms for the amine efficiency under actual, ϕ [—], and dry, ϕ_{dry} [—] conditions:

$$q_{CO2} = \frac{\phi}{\phi_{dry}} f(p_{CO2}, T, \Delta H_{ave}) \tag{2.17}$$

Here f is the temperature and partial pressure-dependent isotherm equation, and ΔH_{ave} [J.mol^{-1}] is the average heat of adsorption calculated in equation 2.17.

$$f_{blocked} = f_{blocked,max}\left(1 - e^{-(kq_{H2O})^n}\right) \tag{2.18}$$

Where $f_{blocked,max}$ [—], k [-], and n [—] are parameters to be fitted.

The model seeks to describe effect (1) with the following equation 2.18. Here, the fraction of the blocked sites by hydrogen-bonded water structures, $f_{blocked}$ [—], is deducted from the theoretical maximum available sites, ϕ_{max} [−], to calculate the fraction of available amine sites for adsorption, $\phi_{\text{available}}$ [—].

$$\phi_{available} = \phi_{max} - f_{blocked} \tag{2.19}$$

The maximum possible amine efficiency, ϕ_{max} [—] is assumed to be 1.

The effect (2), which corresponds to the increase of the stoichiometric ratio due to the formation of ammonium bicarbonate, is described by a Maxwell-Boltzmann distribution, as depicted in Equation 2.20. In a chemical context, this distribution is used to show how, with increase of temperature, a higher proportion of molecular collisions have the required energy for a reaction to occur, such as is described by the Arrhenius Law.

$$\phi = \phi_{dry} + (\phi_{available} - \phi_{dry}) e^{-\frac{A}{q_{H2O}}} \tag{2.20}$$

The value A [mol.kg^{-1}] refers to the critical water loading value. Both parameters A and ϕ_{dry} must be fitted. Lastly, Equation 2.21 attempts to calculate the heat of adsorption, based on effect (3). This is done by measuring a weighted average between the dry and wet states, where ΔH_{dry} [J.mol^{-1}] and ΔH_{wet} [J.mol^{-1}] are the heats of adsorption, respectively. ΔH_{dry} was determined from experimental CO_2 isotherms, whilst $\Delta H_{wet}$is fitted to co-adsorption data. The value of $e^{-\frac{A}{q_{H2O}}}$ corresponds to the fraction of sites that form adsorbed species with water.

$$\Delta H_{ave} = \left(1 - e^{-\frac{A}{q_{H2O}}}\right) \Delta H_{dry} + e^{-\frac{A}{q_{H2O}}} \Delta H_{wet} \tag{2.21}$$

2.4.3 Model Weighted-average dual-site Tóth (WADST)

This approach assumes that there are two types of sites. One with an available water molecule and one without an available water molecule. Furthermore, the same approach as with the mechanistic model will be used to describe the probability that a site has an available water molecule via an Arrhenius style equation described by the same critical water loading parameter A.

$$q_{CO2} = \left(1 - e^{-\frac{A}{q_{H2O}}}\right) \frac{q_{s,dry} b_{dry}(T) P_{CO2}}{\left(1 + (b_{dry}(T) P_{CO2})^{t_{dry}(T)}\right)^{1/t_{dry}(T)}} + e^{-\frac{A}{q_{H2O}}} \frac{q_{s,wet} b_{wet}(T) P_{CO2}}{\left(1 + (b_{wet}(T) P_{CO2})^{t_{wet}(T)}\right)^{1/t_{wet}(T)}} \tag{2.17}$$

Here the dry site in the isotherm is simply defined by the Tóth model shown from 2.2–2.5. Meanwhile, the wet site is again defined by the same equations and fit, alongside A, to co-adsorption experiments, with the dry site already fixed from pure-component isotherms.

2.4.4 Model Stampi-Bombelli

This model was incorporated from the work of Stampi *et al.*, to describe co-adsorption on an amine-functionalized cellulose material by applying an adjustment to the pure Tóth model.

$$q(T, q_{H2O}) = q(T)\left(\frac{1}{1-\gamma q_{H2O}}\right) \tag{2.18}$$

$$b(T, q_{H2O}) = b(T)(1+\beta q_{H2O}) \tag{2.19}$$

The variables γ [—] and β [—] do not have any specific physical meaning but are simply the parameters that describe co-adsorption and should be fit to wet experiments. The authors of this study also suggest that both γ [—] and β [—] should be greater than zero [45].

Figure 2.12 depicts the enhancement factor (q_e/q_{dry}) of co-adsorption experiments performed by Young *et al.* [32], while figure 2.13 shows the data fitting for their two co-adsorption models (Mechanistic and WADST), and for the model from Stampi-Bombelli *et al.* [45], at T= 25 ºC and relative humidity (RH) of 30% and 55%. The parameters found in this fitting process are presented in the Appendix C.3. A few observations can be made: first, no model provides a perfect fit throughout the whole pressure range. While focusing on the lower pressure region, which is the most relevant for our study, very few data points are displayed. The lack of experimental data is not only restricting but can also induce inaccurate fittings for each equilibrium model. Another remark is towards the influence of humidity and partial pressure on adsorption capacity. In picture 2.12 it appears that capacity enhancement follows a decreasing trend along the partial pressure range, to the point when at P_{CO2}= 1 bar, both capacity values at 30% and 55% relative humidity are almost equivalent to dry conditions. Moreover, the effect of relative humidity does not seem to cause adsorption enhancement in isothermal conditions. For the temperature of 25ºC, for example, data points at 30% humidity have superior enhancements when comparing to the 55% relative humidity values.

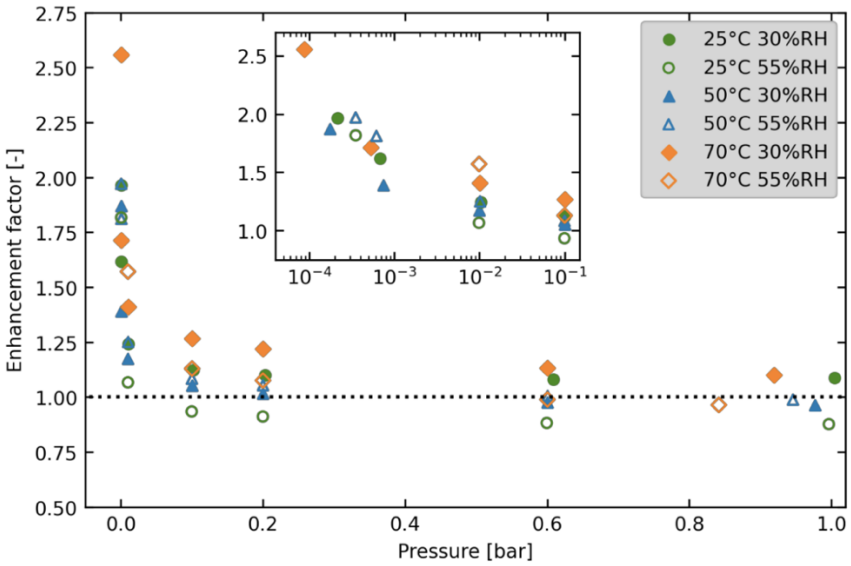

Figure 2.11 - Enhancement factor of co-adsorption experiments by Young et al. [32] plotted against pressure for a range of temperatures and humidity. The enhancement factor is defined as amount of CO_2 adsorbed divided by the amount of CO_2 that would be adsorbed under dry conditions at the same temperature and pressure.

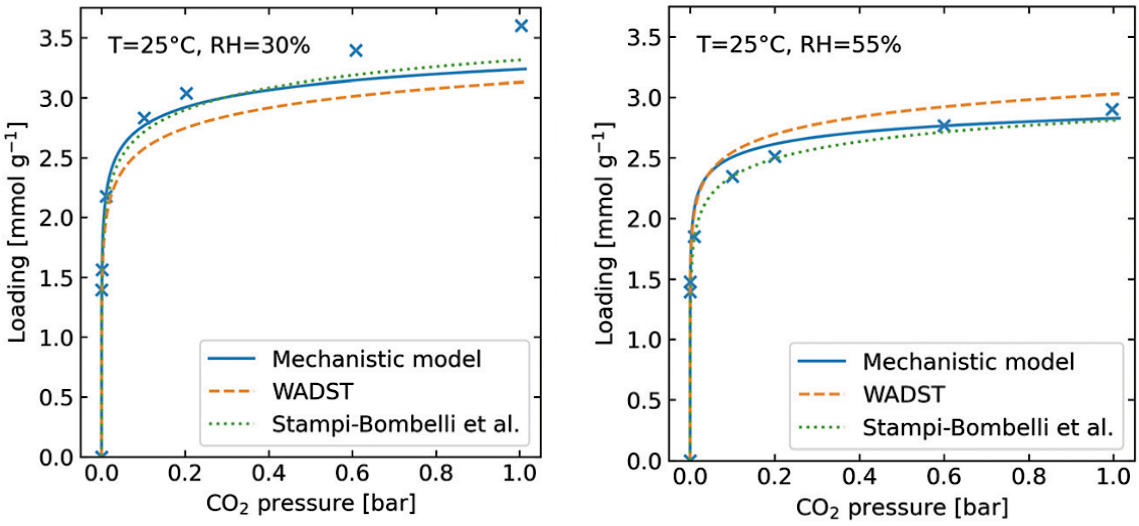

Figure 2.12 - Experimental co-adsorption CO_2 isotherms (markers) at T= 25 ºC and relative humidity (RH) of 30% and 55%, from left to right respectively. All plots were fitted to an empirical literature co-adsorption model from Stampi-Bombelli et al. and the two models from Young et al. [32], comprehended in a pressure range of 0 – 1 bar.

3

METHODOLOGY

To test the mathematical equilibrium models found in previous studies, experiments were performed to obtain the data required to construct adsorption isotherms. The CO_2 capacity was measured for wet air with relative humidity (RH) of 0% - 90% at temperatures 5 – 35 °C, and partial pressures of 40, 200, and 1000 Pa. The dry capacities were measured twice as a reference value to the following measurements under humid conditions. These measurements were featured with previous experimental work done by former bachelor student Marc de Vries [87], who studied as well the effect of water in CO_2 adsorption, in collaboration with the SPT group. The planning of this study's experimental work is described below in Table 3.1.

Table 3.1 - Description of the whole set of experimental data.

P_{CO2} \ T	5ºC	15 ºC	25 ºC	35 ºC
40 Pa				
200 Pa				
1000 Pa				

This work
Marc [87]
Both experiments

3.1 Experimental Apparatus

The setup used for experimental work can be visually described by the photo and scheme below (see Figure 3.1 and 3.2) and focuses on measuring CO_2 adsorption capacities in conditions of direct air capture. It consists of a packed bed reactor, two connected bubble columns referred to as humidifiers, four BROOKS mass flow controllers (MFCs) SLA 5850 series, and a LI-840 gas analyzer (detection range: 0 – 2% CO_2). The gas inlet composition is manipulated by mixing a high purity (grade 5.0) N_2 and CO_2 streams with a N_2 pre-saturated flow, resultant from the humidifier.

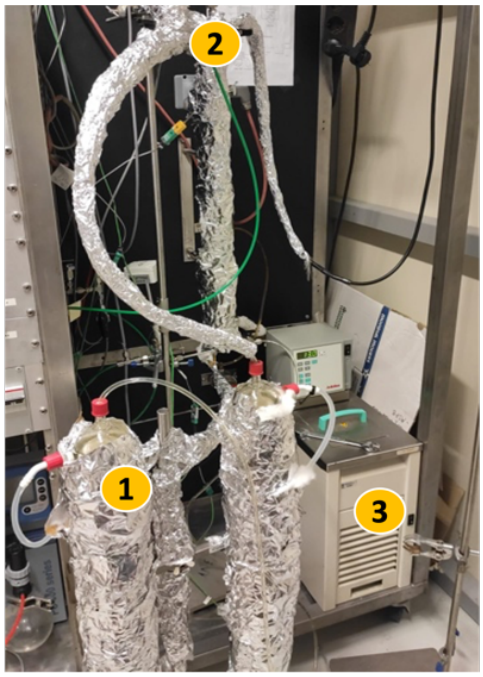

Figure 3.1 – Photo of the experimental setup, including: (1) two humidifiers, (2) a fixed bed adsorption column, and (3) a water bath, as well as the coverage in aluminum foil.

In order to run adsorption experiments over long periods, a water bath JULABO F32/F25 was used to regulate the temperature due to its stability. For the desorption, which was carried out at 90 ºC, the application of an electrical heating Eurotherm 2132 (600W) was considered a far faster option. This is due to the additional time required to cool down the water bath back form desorption to adsorption conditions. Though electrical heating represents higher variability, the risk is outweighed by the small amount of time it takes for the sorbent to regenerate.

An electric tracing at approximately 65 ºC was located between the humidifier and the reactor to heat up to temperatures just above the dew point and prevent possible condensation. Layers of cotton and aluminum foil were also applied around the adsorption column, humidifier, and revolving tubes when simulating conditions at 5 ºC to isolate the setup from the laboratory's ambient temperature.

Temperature monitorization is measured with K-type thermocouples in the axial center of the bed and the inlet and outlet of the reactor. Pressure and humidity sensors were also applied at the reactor entrance and exit.

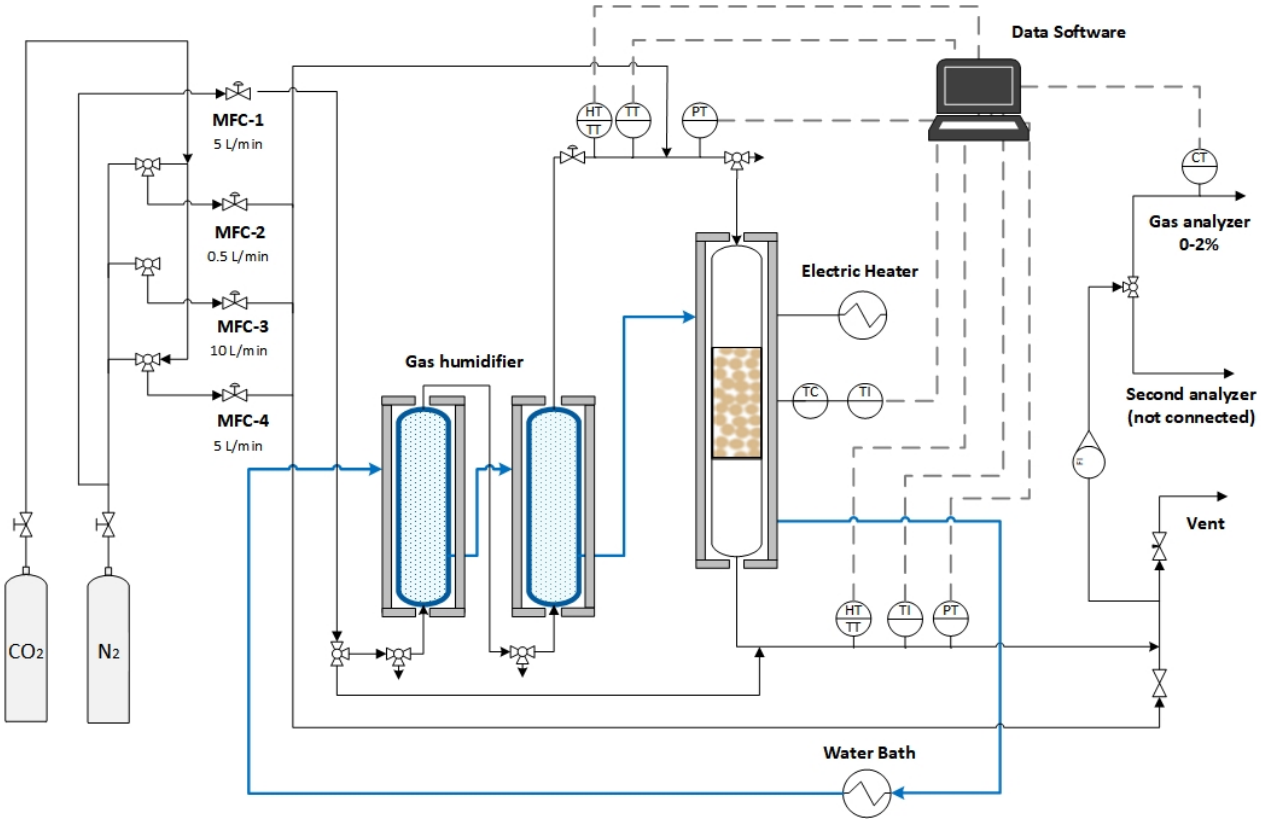

Figure 3.2 - Schematic representation of the adsorption-desorption process setup. The instruments used in the control of the operation's conditions are represented too, such as: MFC (mass flow controllers), HT (humidity transmitter), PT (pressure transmitter), TC (temperature controller). TI (temperature indicator) and TT (temperature transmitter).

3.2 Procedure

The first step of the procedure is to desorb the column to certify that the adsorbent is free from adsorbed molecules. For this, one flushes pure nitrogen from the MFC-4 and sets the electric heater to 90ºC for about an hour. The concentration of 10 ppm was defined as a threshold of what we consider as enough to assume nearly all CO_2 has desorbed. Once that concentration is reached, the electric heater is turned off. We proceed to cool down while running the water bath until the temperature inside the reactor stabilizes. Then, after verifying all the valves and MFC settings, N_2 is fed from MFC-1 through the humidifier and mixed with pure N_2 and CO_2. The gas phase flows through the adsorption column, a fixed bed reactor containing 3.7 g of the solid sorbent inside.

The output data is given by the analyzer that measures the concentration of CO_2 and both ingoing and outgoing temperature, pressure, relative humidity, and bed temperature. Because the analyzer has a limited capacity of 1 $L.min^{-1}$, part of the outlet flow deviates directly to the vents, releasing it into the air. Data points are quantified per second, and the experiment ends a bit after equilibrium is reached, which is described as a steadiness of the sorbent loading. Once it is over, all data is saved, and desorption retakes place.

3.2.1 Breakthrough Method

The experiment is run for a time long enough to reach equilibrium. Each CO_2 concentration in *ppm* is plotted per second to obtain the breakthrough curve. Once it is determined where the plateau was reached, the inlet concentration is achieved by calculating the mean of the last ~3600 data points. The adsorption capacity value is extremely sensitive to this approach, so a meticulous analysis of variations throughout the curve and picking up when equilibrium occurs is critical. Figure 3.3 below represents the resulting breakthrough curves (P_{CO2} = 42.5 Pa) at different temperatures after almost 4 hours, and Figure 3.4 illustrates the inlet and outlet concentrations at the same concentration at T= 15ºC under dry conditions.

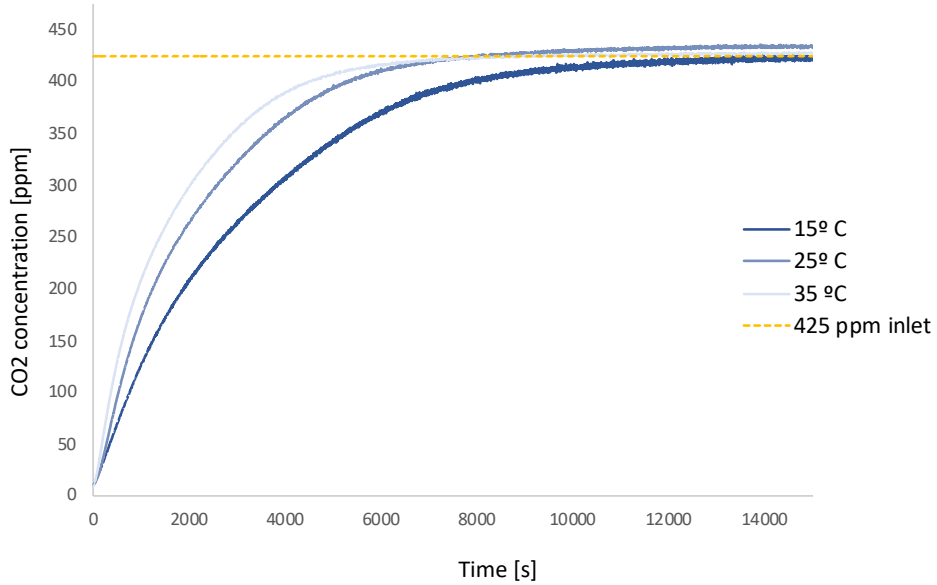

Figure 3.3 - Example of Breakthrough curves at P_{CO2}= 42.5 Pa, in a temperature range 15-35ºC.

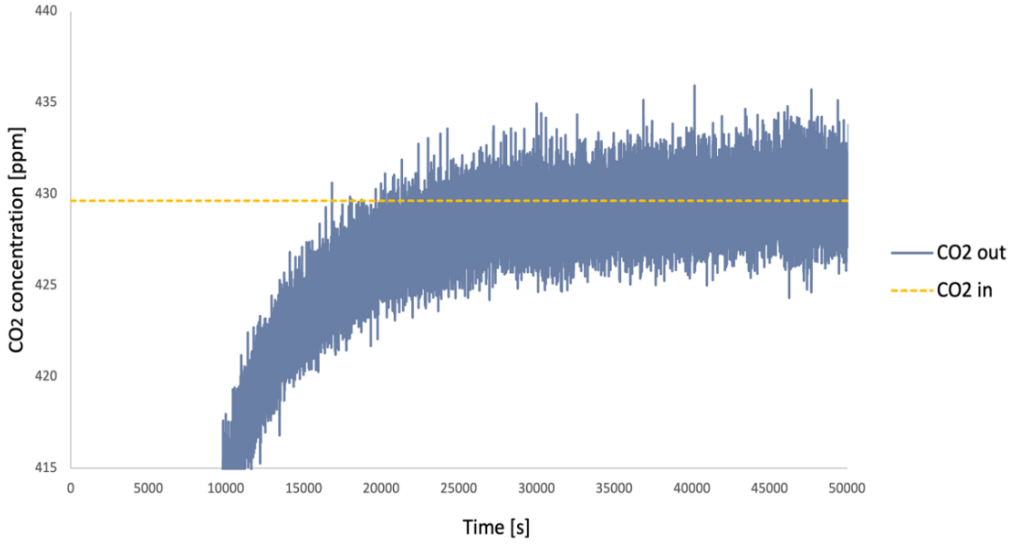

Figure 3.4 – CO_2 concentrations of the inlet and outlet flow, at P_{CO2} = 42.5 Pa, T=15ºC, and 0% RH.

The conversion to sorbent uptake starts by multiplying each inlet and outlet point with the gas molar concentration in $mol.m^{-3}$, M_{gas}, whose value is obtained through the Ideal Gas Law. Then, all data points are multiplied by the total flow rate ($m^3.s^{-1}$), F_v, so that the amount of CO_2 in and out is known (n_{in} and n_{out}, respectively).

$$n = \frac{C_{ppm} M_{gas} F_v}{1e6} \tag{3.1}$$

Using the equation 3.2 below, one can measure how many moles of CO_2 are adsorbed with a subtraction of the outlet and inlet concentration. As the last step, the number of moles is divided by the sorbent mass to get the sorbent loading ($mol.kg^{-1}$), shown in equation 3.3.

$$n_{ads}^{i} = n_{in}^{i} - n_{out}^{i} \tag{3.2}$$

$$q(i) = \frac{1}{m} \int_0^{t=i} n_{ads}^{i} \, dt \tag{3.3}$$

Besides the sorbent capacity, the purpose of these experimental procedures is to obtain the relative humidity (RH) inside the adsorption bed so that it is possible to establish a relationship between CO_2 uptake and moisture. The humidity sensor in the inlet measures the saturated nitrogen from the humidifier. Since CO_2 and dry N_2 are added to the gas composition, and the temperature inside the bed differs from the inlet, this sensor cannot indicate directly the relative humidity inside the adsorption bed.

A few calculations were done for this matter, beginning with Arden Buck's formula, represented in equation 3.4. It correlates saturated vapor pressure with temperature [88], from which we obtain both bed and inlet saturated pressure, based on the temperature output.

$$P_i^{sat} = 0.61121 \exp\left(\frac{18.678 - T_i}{234.5} - \frac{T_i}{257.14 + T_i}\right) \tag{3.4}$$

Afterward, the partial water vapor pressure from the inlet, P_{in}^{W}, is calculated based on the definition of relative humidity, exemplified below. The resulting water vapor pressure is divided by the total pressure measured, leading to the mole fraction of water in the inlet gas, X_{in}^{W}. Both values of RH_{in} and P are given by the output data.

$$P_{in}^{W} = \frac{RH_{in} P_{in}^{sat}}{100} \tag{3.5}$$

$$X_{in}^{W} = \frac{P_{in}^{W}}{P} \tag{3.6}$$

The MFC settings were determined using the volume flow values ($m^3.s^{-1}$) at 100% of its configuration for every experiment. All gas flows (CO_2, dry N_2, and humidified N_2) are considered. The correspondent mixing ratio for each experiment is then determined.

$$mixing\ ratio = \frac{\emptyset_{humid}}{\emptyset_{humid} + \emptyset_{dry}} \tag{3.7}$$

Where $\emptyset$ is the volume flow.

Following the previous results, it just takes multiplying the mixing ratio with X_{in}^{W} to acquire the mole fraction of water present inside the adsorption column, X_{bed}^{W} and, subsequently, the partial vapor pressure of the bed P_{bed}^{wet} (Equation 3.8 and 3.9). The expression 3.10 represents the final equation that leads to the actual RH value (%).

$$X_{bed}^{W} = X_{in}^{W}\ (mixing\ ratio) \tag{3.8}$$

$$P_{bed}^{W} = X_{bed}^{W}\ P \tag{3.9}$$

$$RH = \frac{P_{bed}^{W}}{P_{bed}^{sat}}\ 100 \tag{3.10}$$

As an example of the data obtained from the setup, Figure 3.5 a) and b) represents the bed reactor's relative humidity and temperature, respectively, varying through ~ t = 13.9h at P_{CO2}= 40 Pa, T =15 ºC and the maximum relative humidity of 90 %.

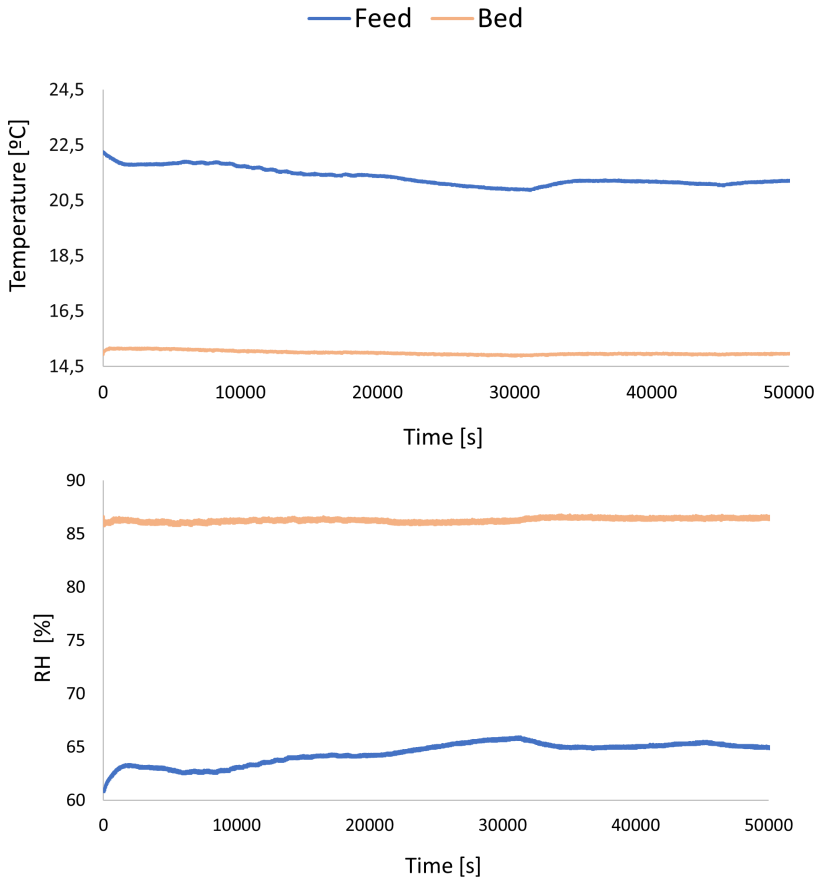

Figure 3.5 – Sample of experimental data from a breakthrough experiment, where the upper picture represents values of the bed temperature (ºC), and the bottom refers to relative humidity (%) at $P_{CO2} = 40$ Pa. Both are result of the same experiment, at 15°C and ~90% relative humidity. Note that the relative humidity of the bed rector was calculated through the equations presented in this chapter.

4

RESULTS AND DISCUSSION

This chapter provides the results of 84 breakthrough experiments that were performed at different values of partial pressure, temperature and relative humidity, as discussed in Chapter 3. The three adsorption models referred in Chapter 2 will be fitted to the experimental data and an empirical model is introduced based on trends of experimental equilibrium capacities.

4.1 Sorbent Stability

In order to validate the method proposed in the experimental chapter, collective breakthrough experiments were performed for the same conditions and compared with each other, in conjunction with the past work of De Vries. When comparing the data from both experiments at P_{CO2} = 40 Pa and temperatures of 15ºC, 25ºC and 35ºC, under dry conditions, the adsorption capacities displayed substantial decreases. The two sets of data are measured around 1-year apart, as presented in Table 4.1 for P_{CO2}= 40 Pa at 15ºC, 25ºC and 35ºC.

Table 4.1 - Experimental data comparison between Marc [87] and this work for P_{CO2}= 40 Pa at 15ºC, 25ºC and 35ºC.

	40 Pa		
	15 ºC	25 ºC	35 ºC
$q_{CO2, Marc}$ [kg.mol^{-1}]	1.18	0.96	0.68
$q_{CO2, me}$ [kg.mol^{-1}]	0.89	0.76	0.56
Difference [%]	24.6	20.8	17.6

The second data set was executed in August of 2021, when the possibility of sorbent degradation came into existence. The set of data points at 15ºC and 25 ºC at 40 Pa from Marc were already incorporated in this study's work, as well as whole set of data for T= 35ºC. Each temperature and partial pressure group of data were repeated under dry conditions, to compare this work's values with the ones obtained before.

The reduction in sorbent loading might be attributed to a few factors such as human-induced error through inconsistent measurements, the setup's environment conditions, i.e., calibration of the mass flow controllers, or sorbent degradation. The human induced error was

first validated by simulating multiple experiments under the same conditions, in order to verify any variability in this work. In Figure 4.1, two separate experiments for P_{CO2} = 40 Pa at T=25 ºC and 0% relative humidity (RH) are presented as a function of sorbent loading through time.

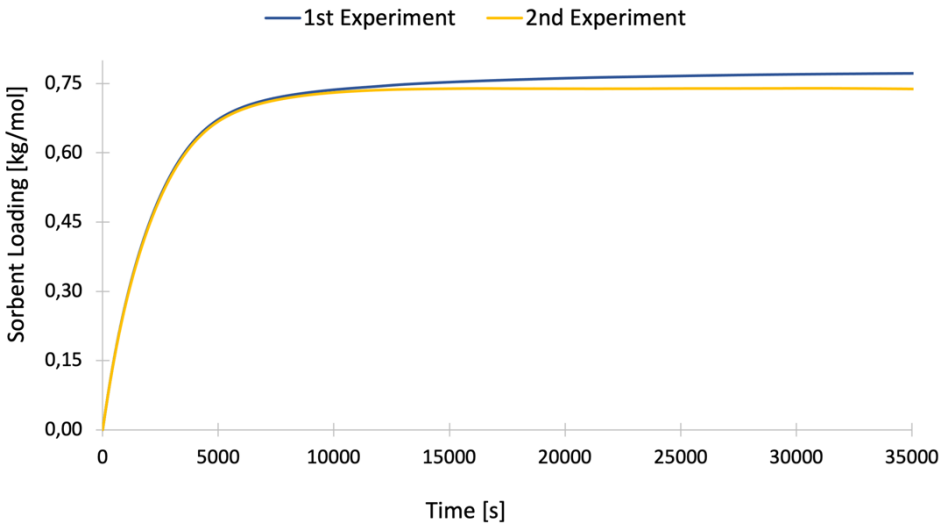

Figure 4.1 - Data confirmation for T=25 ºC and P_{CO2}= 40 Pa. These experiments were performed consecutively, on the 26th and 27th of August 2021. Each adsorption capacity corresponds to 0.77 kg.mol^{-1} (blue) and 0.74 kg.mol^{-1} (yellow).

Although there is some variability within the experiments, it still does not meet the ~20% reduction from Marc's data points. Thus, the second step was to verify if there was an occurrence of sorbent degradation, despite previous studies with Lewatit claiming its endurance and thermal stability. In order to confirm it, TGA was applied as an alternative to the breakthrough method. Thermo-gravimetric analysis (TGA) is used to determine sorbent capacity by measuring the mass increase by passing a gas stream of a non-adsorbing gas like N_2, containing a known amount CO_2. Once desorption takes place and temperature increases, the sorbent will release CO_2 and the sample mass decreases again. The capacity can then be determined by both the adsorption step as well as the desorption step in the TGA [57].

A TGA measurement was performed at 40ºC and 15% CO_2 under dry conditions. The resulting capacity was 1.59 mol.kg^{-1}. Alternatively, the known isotherm value for these conditions is equivalent to 2.39 mol.kg^{-1}, which means a 34% reduction. However, the "fresh" sorbent used in this study does not have the same quality as sorbent used to measure the literature isotherm value, which is approximately 17% less [89]. That means that the degradation within experiments seems to suggest a reduction around 20%.

Figure 4.2 illustrates the plotting of experimental adsorption capacities throughout air's relative humidity. At first sight, one can tell that the original data from Marc de Vries [44] at 15 ºC and 35 ºC (dashed lines) are laying very closely to the capacities corresponding to lower temperatures, 5 ºC and 25 ºC, respectively. Bearing in mind that his values are superior to the ones measured in this work, the actual position of these lines should be lower. After applying

a 20% degradation factor to his values (straight lines), a more even spacing is perceptible between each temperature's data, which appears more realistic.

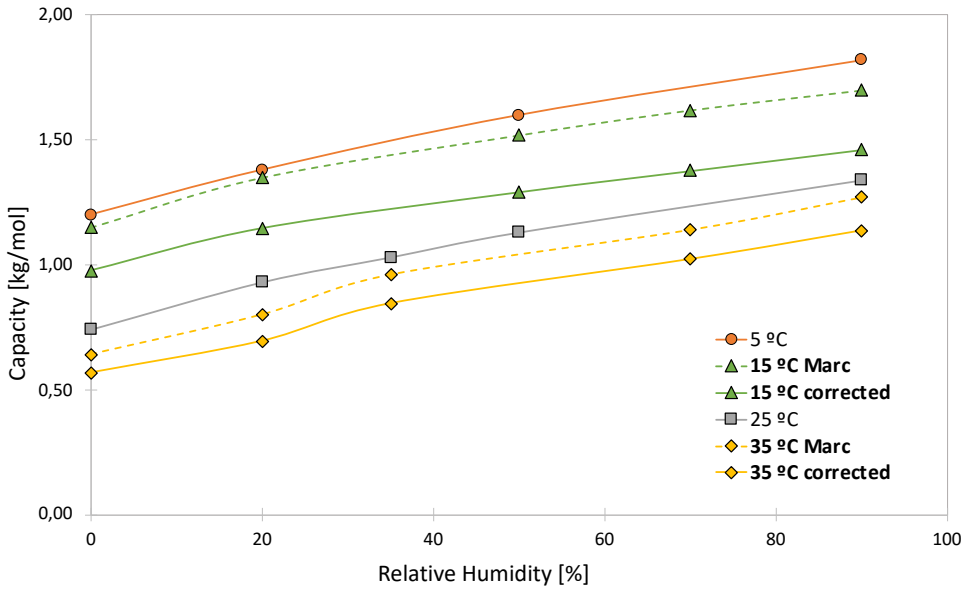

Figure 4.2 - Experiments from this work and Marc's at P_{CO2} = 40 Pa, being Marc's data 15ºC and 35ºC. From upper to bottom: a) experimental data with no reduction factor; b) Experimental data with a 20% reduction factor.

While the capacity difference was calculated merely for dry conditions, it is inevitable the possibility of inaccuracy when applying that same percentage to humid experimental values, which can have a lower or higher degradation level. Regardless of its validity, the same "correction" factor was introduced to the remaining data incorporated from Marc's experiments (see Table 3.1 in Chapter 3), as time was too limited to cover the whole range of relative humidity.

4.2 Experimental Trends

The whole set of experiments of the current work is shown in Figure 4.3, as a function of adsorption capacity against relative humidity. The three plots are divided into different CO_2 partial pressure sets: 40 Pa, 200 Pa and 1000 Pa.

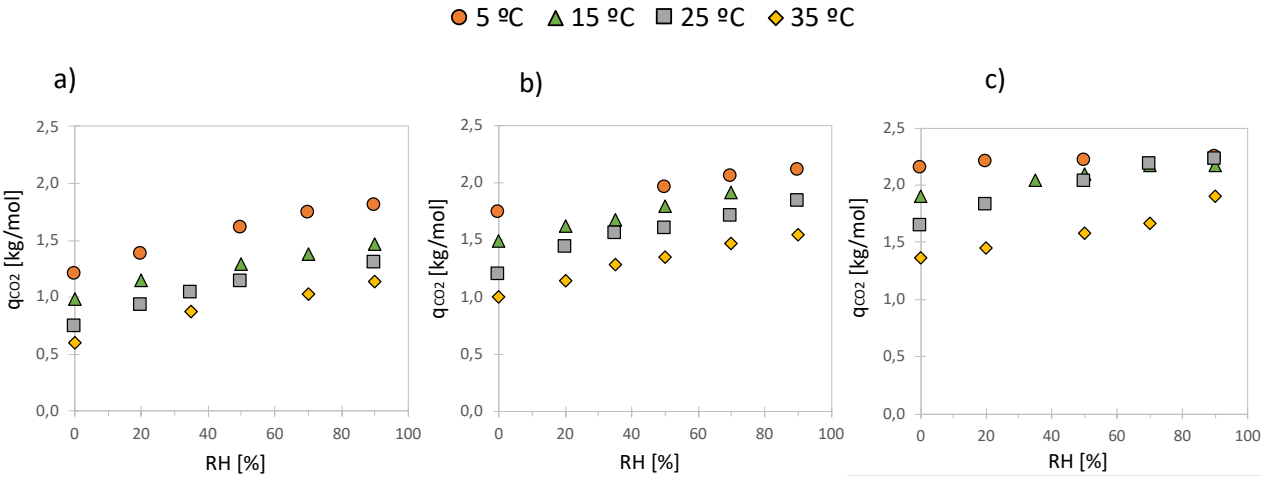

Figure 4.3 - Results of CO_2 adsorption equilibrium data at different temperatures and partial pressures, throughout relative humidity, using the breakthrough method. From left to right: a) 40 Pa; b) 200 Pa; c) 1000 Pa.

It was found that the total adsorption-desorption cycle time decreases with increased column temperature and feed rates. Longer adsorption periods at lower temperatures were needed to attain equilibrium compared to higher temperatures. The lowest temperatures were also found to have the highest adsorption capacity, as expected from the exothermic nature of the adsorption process. The lower the temperature of the gas is, the lower will be the kinetic energy of gas and hence particles will move slower. The particles moving with less speed have increased attractive forces between them, so the lower temperature favors physical adsorption. Nevertheless, not all data displays a consistent linear trend with temperature. In fact, at higher CO_2 feed rates (P_{CO2}=1000 Pa), the temperature trends displayed similar capacities, particularly at the higher range of relative humidity (RH). From observation of the overall data, the 35ºC, 25ºC and 15ºC are the sets with least irregularities in adsorption trends. It is possible that this is due to the ambient temperature of the setup, while the 5ºC set had bigger temperature variabilities, despite the addition of cotton isolating layers.

While considering the effect of different CO_2 partial pressures, CO_2 adsorption capacity was found to be increased with the CO_2 concentration present in the gas stream. At P_{CO2}= 40 Pa, the maximum loading corresponds to 1.82 kg.mol^{-1}, while at P_{CO2}=1000 Pa, the highest capacity is 2.25 kg.mol^{-1}.

The maximum amount of CO_2 adsorbed/kg of the adsorbent of the whole experimental set was 2.25 kg.mol^{-1} (P_{CO2}= 1000 Pa, T= 5ºC, RH= 84.97%), which is inferior to the maximum value reported in literature. Bearing in mind that these values are lower (approximately 20%) than the standard ones, the maximum value would reach ~2.7 mol.kg^{-1}, which is significantly closer to the highest literature value, i.e., 2.95 mol.kg^{-1} (see section 2.2.1).

Lastly, sorbent loading behavior in presence of water vapor is seen to be improved, particularly in the lower partial pressure experiments. As it is both challenging and imprecise to compare the influence of humidity throughout the whole experimental results, based solely in observation of the plots depicted in Figure 4.3, another representation form is presented in this

chapter. Figure 4.4 displays the calculated capacity enhancement, in the form of equilibrium capacity divided by the respective experimental dry value (q/q_{dry}), plotted against relative humidity. Through these calculations, it is possible to quantify how much difference the humidity brings to equilibrium capacity.

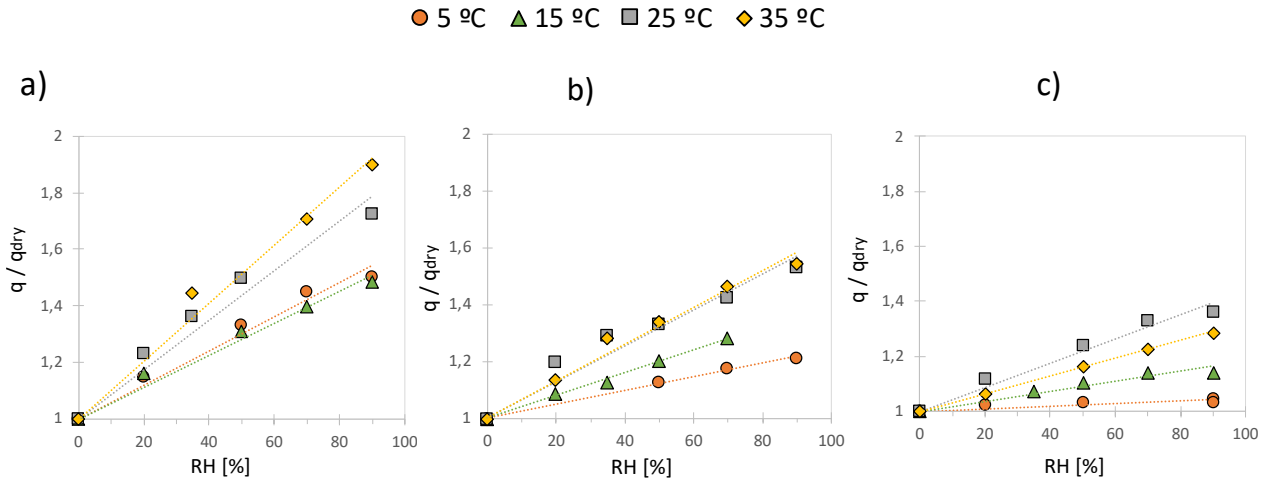

Figure 4.4 - Plots of the enhancement factor of co-adsorption experiments against relative humidity, at different temperatures and partial pressures. From left to right: a) 40 Pa; b) 200 Pa; c) 1000 Pa.

It is confirmed that capacity is enhanced largely in lower partial pressure ranges. At P_{CO2}= 40 Pa and T= 35ºC, the capacity adsorption nearly doubled in presence of high moisture content (q_{dry}= 0.60 kg.mol^{-1}, q_{humid}= 1.07 kg.mol^{-1}, RH=90%). On the other hand, at the highest partial pressure set of experiments (P_{CO2}= 1000 Pa), humidity seems to have a reduced impact on the adsorption capacity. Indeed, the lowest enhancement corresponds to P_{CO2}= 1000 Pa and T= 5ºC, whose variance is nearly none. Gebald *et al.* [78] also observed this phenomenon, as described in section 2.3.3, while some even witnessed a decrease in capacity in presence of elevated concentrations of CO_2 and water in the gas stream [80].

Young *et al.* [32] and Buijs and De Flart [30] have also observed this phenomena, raising the hypothesis that carbamic acid formation is the main adsorption mechanism on Lewatit VP OC 1065, as mentioned before in section 2.3.3. The reason for this is due to the inconsistent capacity enhancement throughout the whole CO_2 partial pressure range, as opposed to the 2:1 stoichiometric ratio described by ammonium bicarbonate (or hydronium carbamate) formation.

As opposed to the temperature behavior observed in the previous figure, here the enhancement is seemingly boosted by higher temperatures. Temperatures within the range of 35ºC and 25ºC have the highest differences from its dry capacity, while temperatures between 15ºC and 5ºC show little enhancement ($q/q_{dry} \leq 1.5$). The temperature trends warrant some discussion. The two pairs of temperatures alternate between each other, making the trends not very clear. This might be due to the high complexity associated with adsorption mechanisms. Furthermore, the possibility of experimental mistakes linked to the dry values cannot be

dismissed, which could have an impact on the humid values, and subsequently, capacity enhancement.

To summarize, the conditions intrinsic to ambient air ($P_{CO2} \cong 40$ Pa and presence of moisture) seem to serve advantageously CO_2 sequestration. It's within that range that the presence of water has the highest enhancement and the highest adsorption capacities. Temperature wise, the lowest temperatures are the ones with higher adsorption loadings but are the least affected by the presence of water. Higher temperatures, on the other hand, can nearly double its capacity in its presence. Looking into it from a real-DAC setting perspective, the presence of water in air only proves to be beneficial to a certain extent. For example, if the adsorption process is operated at low temperatures, the enhancement in presence of high levels of humidity is almost none, while still being affected by the energy penalty associated.

4.3 Equilibrium Models

There are two types of data analysis, graphical and numerical. Graphical measures allow the reader to view the entire data set at once, as they can easily display a wide range of relations between the model and the data. Numerical measures, on the other hand, are more narrowly focused on a particular aspect of the data and tend to compress that information into a single number [90]. Therefore, both types of analysis are going to be presented to discuss the performance of each fit.

To validate each equilibrium model based in literature, in the context of this work, parameter fitting was calculated using the *fminsearch* function provided by MATLAB®, in combination with multiple starting points. The function is designed to find a minimum of a scalar function of several variables, starting at an initial estimate. Through some trials of initial values for each parameter, the Sum of Square Errors (SSR) was calculated for each fitting, which would correspond to the lowest value resultant from *fminsearch*. This statistic measures the total deviation of the response values from the fit to the response values. A value closer to 0 indicates that the model has a smaller random error component, and that the fit will be more useful for prediction [90]. Afterwards, the squared difference between the observed dependent variable and the mean of experimental data was calculated (SST) to obtain the R-squared of each equilibrium model. The SSR assesses how well the model represents the fitted data, while SST measures the variability in the data used in the regression model [91]. R^2 is the square of the correlation between the response values and the predicted response values. For the same data set, higher R-squared values represent smaller differences (variance) between the observed data and the fitted values [92]. Both SSR, SST and R^2 are represented in Equation 4.1.

$$R^2 = \frac{SSR}{SST} = \frac{\sum(\hat{y}_i - \bar{y})^2}{\sum(y_i - \bar{y})^2} \tag{4.1}$$

The R^2, however, does not explain the relationship between the dependent and the independent variables. It also does not inform about the quality of the regression model, as residual plots are not assessed. To compare the fitting between all models, a visual analysis of all fittings is going to be implemented.

4.3.1 CO_2 Adsorption under Dry Conditions

The plot from the fitting of the Tóth equilibrium model is represented in Figure 4.5, next to the correspondent experimental data. As expected, the Tóth model shows a good fit to the data with a high coefficient of determination ($R^2 > 0.99$), described in Table 4.2. The disparity plot, presented in Figure 4.6, enforces the premise that experimental data follows the same trends fitted by the equilibrium model. Nonetheless, the accuracy of the parameters calculated for this model is still limited by the reduced sample size, which in turn allows an easier fitting.

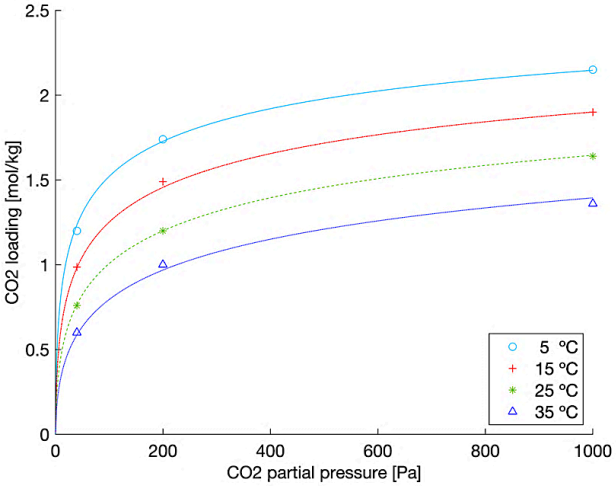

Figure 4.5 - Temperature dependent isotherm model and experimental data.

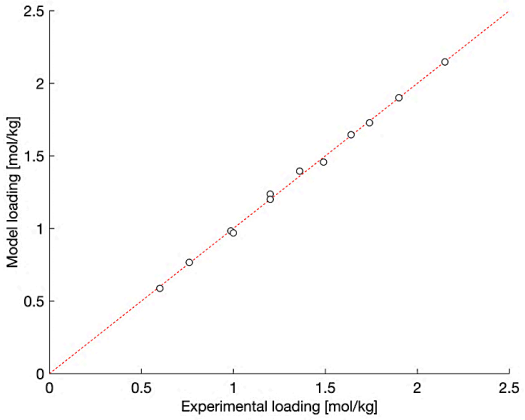

Figure 4.6 - Parity plot of the temperature dependent Tóth model, with both experimental and fitted values of dry adsorption conditions.

Table 4.2 - Fitting parameters of the temperature dependent Tóth isotherm model.

Tóth Model	
q_{s0} [mol.kg^{-1}]	2.761
χ [-]	0
T_0 [K]	298.15
b_0 [Pa^{-1}]	3.297E-06
ΔH_{ads} [J.mol^{-1}]	2.615E+04
t_0 [-]	0.342
α [-]	-0.793
SSR	0.006
R^2	0.998

From all parameters from the Tóth equilibrium model, q_{s0} is the one with the most coherent physical meaning, referring to the maximum equilibrium loading. The value obtained from the Tóth fit, $q_{e,CO2\ work}$=2.761 mol.kg^{-1}, is close to the one fitted previously for CO_2 adsorption over Lewatit, $q_{e,\ CO2}$ = 3.4 mol.kg^{-1} [27], [36], and the maximum experimental capacity from this work, 2.25 kg.mol^{-1} (or $q_{e,\ CO2}$ = 2.70 mol.kg^{-1} at the sorbent's full capacity). It is also concordant with the maximum capacity measured experimentally with Lewatit, 2.95 mol.kg^{-1} [53]. Here, the reference temperature (T_0) was assumed to be 298.15 K, considering that the experiments were operated in ambient conditions. The heterogeneity parameter at reference temperature, t_0,was found to be extremely close to previous fitted values, from Veneman and Bos (see Appendix C.1). While comparing values from this work to others, the highest difference corresponds to the equilibrium parameter, b_0, which is significantly smaller. The same parameter was observed to be highly sensitive to initial estimates in MATLAB.

4.3.2 CO_2 Adsorption under Humid Conditions

The parameters resultant from the fitting process are presented in Table 4.3. Figure 4.7 shows the fit of the experimental data, alongside the two co-adsorption models from Young et *al.* [32], and the model from Stampi-Bombelli *et al.* [45], and an empirical model based on the experimental values, which will be later presented in this chapter. The fitting of the three models in Figure 4.7 is at a fixed temperature of 25ºC, with three different CO_2 partial pressures, against humidity. The remaining temperatures are presented in Appendix D.1, as well as the disparity plots of each equilibrium model and the respective fitted parameters found in literature.

Table 4.3 – Fitted parameters of the co-adsorption models Mechanistic, WADST and Stampi-Bombelli.

Mechanistic Model	
A [mol.kg^{-1}]	1.733
ϕ_{dry} [-]	0.429
$f_{blocked}$ [-]	0.605
k [-]	0.097
n [-]	27.577
ΔH_{ads} [J.mol^{-1}]	3,247E+04
SSR	0.403
R^2	0.964
WADST Model	
$q_{s0,wet}$ [mol.kg^{-1}]	4.591
$\chi_{,wet}$ [-]	0.031
$b_{0,wet}$ [Pa^{-1}]	1.239E-05
$\Delta H_{ads,wet}$ [J.mol^{-1}]	5.113E+04
$t_{0,wet}$ [-]	0.136
$\alpha_{,wet}$ [-]	-1.502E-04
A [mol.kg^{-1}]	1.723
SSR	0.360
R^2	0.968
Stampi-Bombelli Model	
β [-]	0.814
γ [-]	-0,006
SSR	0.338
R^2	0.969

a)

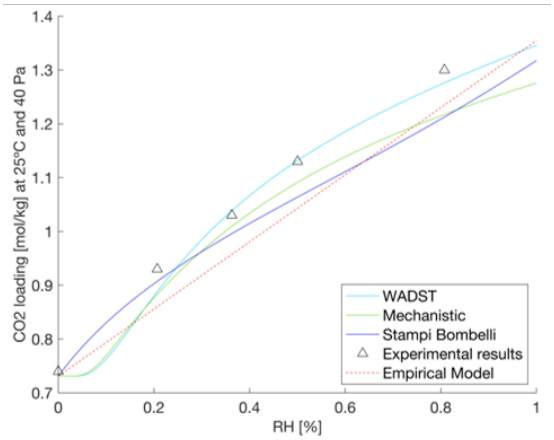

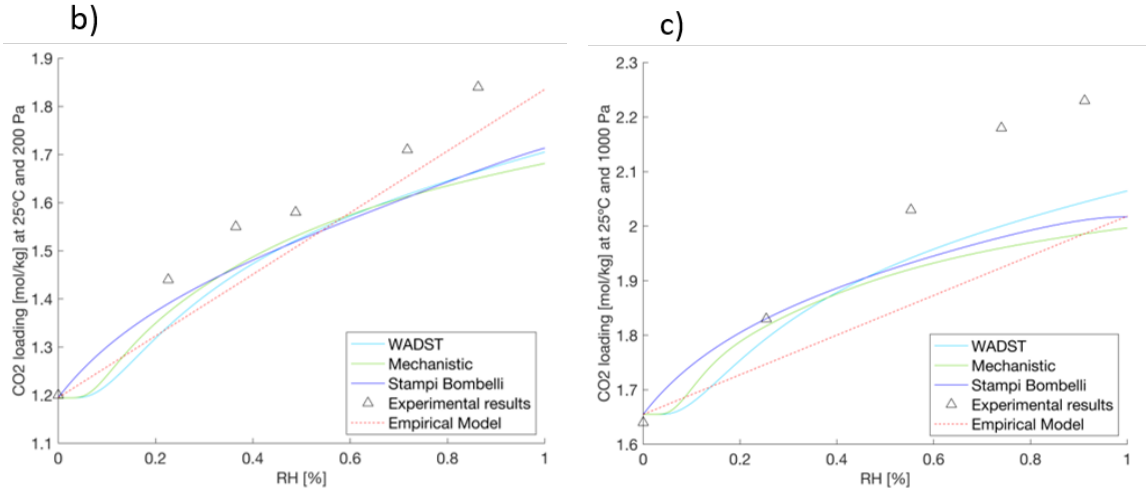

Figure 4.7 – Representation of the three models found in literature, plus a proposed empirical model based on the experimental values. The three plots are at the same temperature of 25ºC, being a) 40 Pa, b) 200 Pa, and c) 1000 Pa.

The parameter ϕ_{dry} [-] in the Mechanistic model was fitted as 0.429, as opposed to the value of 1 fitted by the author Young *et al.* [32]. From this study's outlook, the stoichiometry under dry conditions corresponds to approximately half of the value under wet conditions. The latter phenomenon can be described by both ammonium bicarbonate and hydronium carbamate reaction, suggesting its formation in CO_2 adsorption in presence of water.

The author also implied that the critical water loading parameter, A, has a similar value for both Mechanistic and WADST model. The same occurrence is found in this work, which corresponds to 1.733 mol.kg^{-1} and 1.723 kg.mol^{-1}, respectively. This might imply that both models predict the same probability of a CO_2 adsorption site having a water molecule available given the same loading of water. The fitting presented in the WADST model for q_W corresponds to 4.591 mol.kg^{-1}, which turns to be significantly smaller than the fitted values of Young *et al.* [32] (q_W = 9.035 mol.kg^{-1}), and the maximum CO_2 capacity under humid conditions, reported experimentally by Garcia Martinez [43] (q_W=18.5 mol.kg^{-1}, RH=93%, T=21.7ºC).

A significant matter to be denoted is that no model provides a perfect fit, and there is at least one case for each model where a relatively poor fit is found, reinforcing the high complexity associated to co-adsorption mechanisms. From a graphical analysis, the WADST model seems to have the closest fit, particularly at P_{CO2}= 40 Pa. Looking at the numerical evaluation of the fit, the Stampi-Bombelli model shows both the lowest SSR and the highest R-squared, which is relatively close the fit applied to the WADST model.

The three models, overall, fit better in the lower pressure range, and for DAC conditions (i.e., P_{CO2} = 40 Pa) and at temperatures of 15 ºC and 25 ºC. The temperature conditions might be due to the experimental data itself. Since these two sets of temperatures were the ones that had a more consistent behavior, it might justify why the fitting was closer to the data trends.

4.3.3 Empirical Model

The models presented by literature did not display a reliable fit to the experimental data, within the complete range of conditions. Precisely for this reason, an equilibrium adsorption model was developed to mathematically describe experimental trends from this work.

The foundation for the proposed model will be the Tóth isotherm, as it has been observed that it describes well CO_2 adsorption under dry conditions. The next step is to identify which type of behavior the CO_2 capacity enhancement follows in the presence of water. The exact parameters are not the focus, the type of function is. Most plots presented in Figure 4.4 illustrate a linear trend throughout the relative humidity array, while other trends decrease in capacity enhancement at higher values of humidity, which could be better described by a 2nd degree polynomial function. However, the resultant slopes did not show a clear trend, which caused this type of function to be dismissed. Subsequently, the linear function ($y = mx + b$) was chosen to represent the humidity enhancement, being the y-intercept b=1, and the dependable variable x correspondent to relative humidity (RH). The equation is defined in 4.2 and 4.3.

$$\frac{q_{humid}}{q_{dry}} = \left[a\left(T, P_{CO_2}\right)RH\right] + 1 \tag{4.2}$$

$$q_{humid} = q_{dry} * \left\{\left[a\left(T, P_{CO_2}\right)RH\right] + 1\right\} \tag{4.3}$$

To describe the effect of temperature and partial pressure, $a = f(\mathrm{T}, \mathrm{P_{CO2}})$, the first step was to plot the slopes of the different capacity enhancements against temperature, as shown in Figure 4.8. The resultant trends demonstrate that high partial pressures (i.e., 200 and 1000 Pa) decrease its slope at higher values of temperature, which has also been observed in experimental results. Nonetheless, for the sake of practicality, a linear function was applied too, to portray the behavior of a versus temperature. For future reference, the behavior of capacity enhancement ($\mathrm{q/q_{dry}}$) is better described by a polynomial function than by a linear function. Here, $a\left(T, P_{CO_2}\right)$ is described by equation 4.4, where the dependent variable is temperature [K]. Both slope and y-intercept, c [-] and d [-] respectively, are partial pressure dependent variables that require fitting.

$$a\left(T, P_{CO_2}\right) = (cT) + d \tag{4.4}$$

Figure 4.8 displays that the slopes of $\mathrm{q/q_{dry}}$ at $\mathrm{P_{CO2}}$= 200 Pa do not follow the same behavior throughout temperature as the remaining trendlines, considering that capacity value at T= 5ºC is considerably high when comparing with other partial pressures. The fitting for c [-]and d [-] is calculated through plotting the slope and y-intercept from each linear function,

against partial pressure (see Figure 4.9). The best fit for both resulted in logarithmic function, as expressed by Equation 4.5 and 4.6.

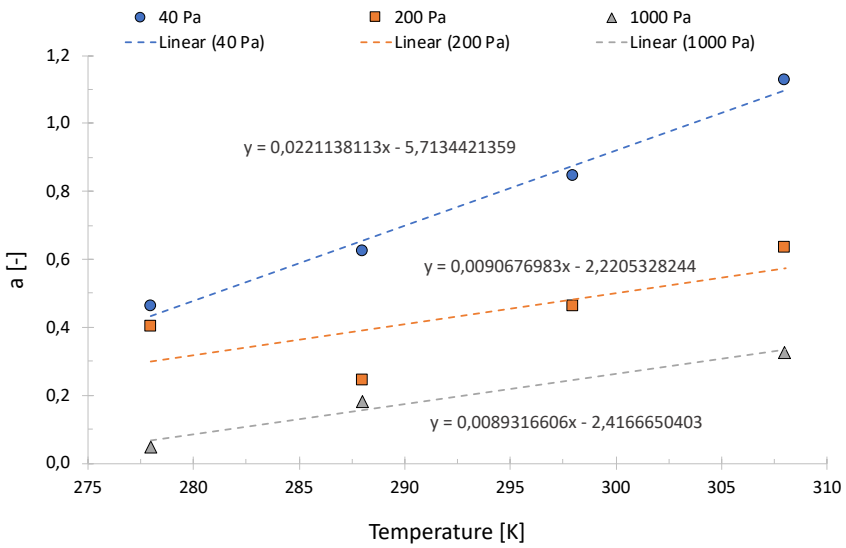

Figure 4.8 - Plot of the different slopes of capacity enhancements [-] against temperature [K].

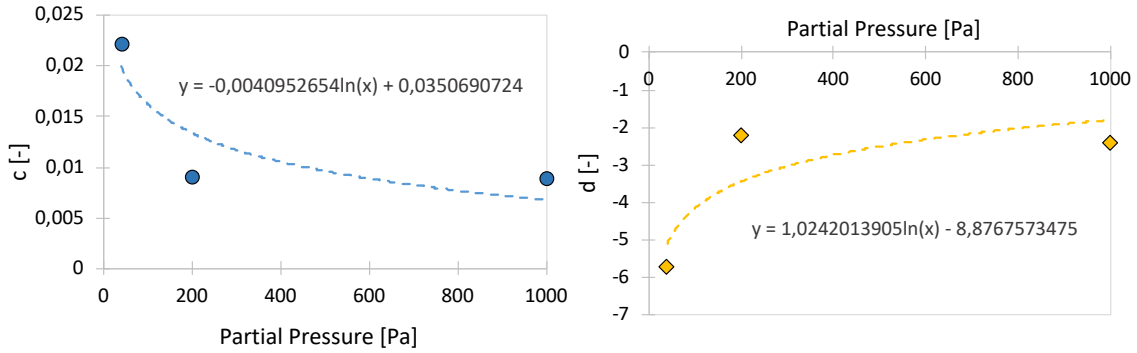

Figure 4.9 - Plots of the different slopes [-] and y-intercepts [-], from left to right, against partial pressure [Pa].

$$c = e\ln\left(P_{CO_2}\right) + f \tag{4.5}$$

$$d = g\ln\left(P_{CO_2}\right) + h \tag{4.6}$$

The empirical model is represented beforehand in Figure 4.7 (red dashed lines), along with the other equilibrium models from literature, against relative humidity (RH). Because it is designed as a linear function, it does not follow the curve that results from a stagnation in capacity enhancement at high levels of relative humidity, as it is observed in experimental data. Furthermore, a disparity plot is presented in Figure 4.10 below, describing the capacity gap between experimental values and the ones obtained through this model for the same conditions, with the blue and green dashed lines being a 10% deviation. It is easily noticeable that many values from the Empirical model are located beyond the range. This translates into great disparity between the two sets of data and, consequently, poor model conceptualization and

fitting. A further observation is that the model has a higher accuracy within a lower partial pressure range, which comes in conformity with the fitting of the other three equilibrium models found in literature. The results are presented in Table 4.2, in which both SSR and R^2 values analytically validate previous statements, i.e., R^2<0.9 and the SSR value is the highest from all the co-adsorption models, which corresponds to a poor fitting.

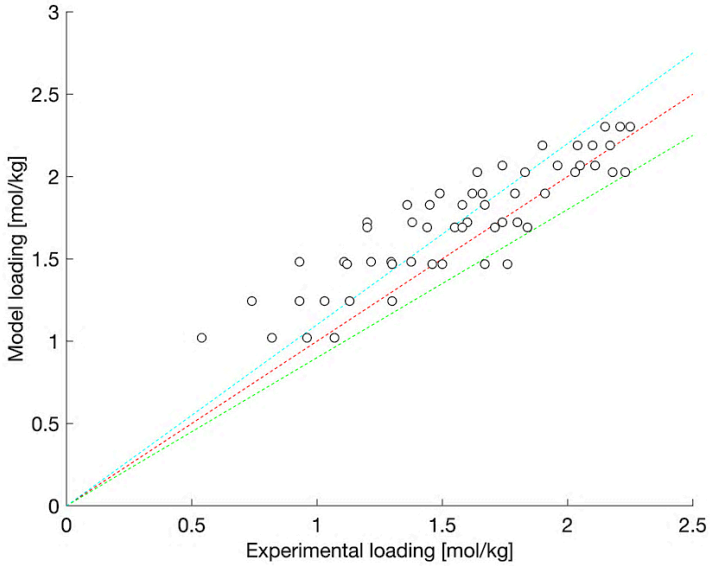

Figure 4.10 - Disparity plot between the empirical model and experimental adsorption capacities

Table 4.4 - Fitted parameters of the co-adsorption empirical model.

Empirical Model	
e [-]	-4.095e-03
f [-]	3.507e-02
g [-]	1.024
h [-]	-8.876
SSR	0.801
R^2	0.657

5

CONCLUSIONS AND FUTURE WORK

5.1 Conclusions

Adsorption experiments were executed under broad ranges of humidity, temperature and concentrations of CO_2, in order to analyze how each parameter influences CO_2 capture directly from ambient air (DAC), on a supported amine sorbent. For this, all sets of data were analyzed to verify the existence of any trend. The same values were then applied to models already developed from a mechanistic understanding and compared within each fit.

The measurements were performed by application of the breakthrough method on a pilot scale setup, with a fixed bed adsorption column, in the facilities of the Sustainable Process Technology (SPT) department. These were featured with previous experimental work done by a student from the SPT group, Marc de Vries, who covered too the effect of water in CO_2 adsorption. After performing 84 breakthrough experiments and comparing both sets of data, it was concluded that the sorbent material might had suffered ~20% degradation, due the decrease in capacity under similar conditions. In response to that possibility, a correction factor was applied into previous values.

The maximum amount of CO_2 adsorbed/kg of the adsorbent of the whole experimental set was 2.25 $kg.mol^{-1}$ (P_{CO2}= 1000 Pa, T= 5ºC, RH= 84.97%), and ~2.7 $mol.kg^{-1}$ after the correction factor, which is significantly close to other values found in literature. At P_{CO2}= 40 Pa and T= 35ºC, the capacity adsorption nearly doubled in presence of high moisture content (q_{dry}= 0.60 $kg.mol^{-1}$, q_{humid}= 1.07 $kg.mol^{-1}$, RH=90%). At the highest partial pressure set of experiments (P_{CO2}= 1000 Pa), on the other hand, humidity seems to have a reduced impact on the adsorption capacity. Overall, the CO_2 equilibrium loading increases with relative humidity (RH) in all data sets. It was also observed that the lowest temperatures are the ones with higher adsorption loadings but are the least enhanced in presence of moisture.

In general, the conditions intrinsic to ambient air ($P_{CO2} \cong$ 40 Pa and presence of moisture) seem to serve favorably CO_2 capture. However, due to the high complexity of co-adsorption mechanisms and the application of a degradation factor, some results displayed some inconsistency in its trends.

The CO_2 adsorption data from this work, when compared with the existent equilibrium models, showed both good and poor agreements depending on the conditions. The Tóth isotherm model describes well the experimental results throughout the whole temperature (T) and partial pressure (P_{CO2}) range, whose fitted values come in accordance with its physical implication and with values found in literature. For DAC conditions, experimental trends were well characterized, which follows literature remarks. In summary, the WADST and Stampi-Bombelli model were the co-adsorption models that represented closest fits, from graphical and numerical analysis. On the other hand, the empirical model that was also

proposed based on the observation of experimental trends showed poor fitting, which might be due to the choice of a linear function to represent the capacity enhancement.

Another remark is that the experimental data has sources of potential error. Firstly, the use of the degradation factor might have compromised the data, as it is not making use of the sorbent's full capacity potential, nor considering the degradation under the presence of water. Secondly, this work is trying to elucidate the effect of three parameters (temperature, pressure, and humidity) at once, and there is a possibility for measurement error in all these. Considering this, it should not be expected that the models are be able to fit the experimental values.

Nevertheless, the results obtained in this study constitute an important addition of data to the studies on direct air capture, as they are yet in an early stage. The research gaps for the study of CO_2 - H_2O interaction, in these conditions, constitute an obstacle to be overcome in order to understand its mechanisms, and subsequently, implement a more efficient system of CO_2 capture from ambient air.

5.2 Future work

As there are great uncertainties regarding the obtained values, the first and main recommendation would be to further investigate the degradation at humid conditions and to perform additional validation experiments for the "older" data.

It is also strongly suggested to reinforce temperature and relative humidity stability throughout adsorption experiments. Results showed that room-temperature displayed better conformity with each other, as opposed to the ones correspondent to 5ºC. This could be reached through a stricter control of the room's ventilation and/or implementing a stronger thermal isolation material around the setup.

Additional analytical technics are recommended as well to understand the adsorption mechanisms and its species formed under the presence of water. For instance, through spectroscopy measurements such as NMR and FTIR, it is possible to study the resultant substances at a molecular level. For Lewatit VP OC, in particular, more research under a wide range of conditions (RH, T and P_{CO2}) is needed to confirm previous hypothesis that no ammonium bicarbonate is formed (see section 2.3.3.), and if such is established, set which ones are possibly formed instead.

Conclusively, when developing an equilibrium model based on experimental trends, an alternative type of function for CO_2 capacity enhancement behavior is should be considered. The polynomial-type seemed to describe closer this work's results.

REFERENCES

[1] Dutcher, B.; Fan, M.; Russell, A. G. Amine-Based CO2 Capture Technology Development from the Beginning of 2013—A Review. *ACS Appl. Mater. Interfaces* **2015**, *7* (4), 2137–2148. https://doi.org/10.1021/am507465f.

[2] Cook, J.; Oreskes, N.; Doran, P. T.; Anderegg, W. R. L.; Verheggen, B.; Maibach, E. W.; Carlton, J. S.; Lewandowsky, S.; Skuce, A. G.; Green, S. A.; Nuccitelli, D.; Jacobs, P.; Richardson, M.; Winkler, B.; Painting, R.; Rice, K. Consensus on Consensus: A Synthesis of Consensus Estimates on Human-Caused Global Warming. *Environ. Res. Lett.* **2016**, *11* (4), 048002. https://doi.org/10.1088/1748-9326/11/4/048002.

[3] Sterman, J. D.; Sweeney, L. B. Cloudy Skies: Assessing Public Understanding of Global Warming. *Syst. Dyn. Rev.* **2002**, *18* (2), 207–240. https://doi.org/10.1002/sdr.242.

[4] Stein, T. Carbon Dioxide Peaks Near 420 Parts per Million at Mauna Loa Observatory. *NOAA Global Monitoring Laboratory*. **2021**.

[5] EASAC. *Negative Emission Technologies: What Role in Meeting Paris Agreement Targets?*. Halle, 2018. Policy Report.

[6] NASA. Scientific Consensus: Earth's Climate Is Warming. *Global Climate Change*, **2022**. https://climate.nasa.gov/scientific-consensus/ (accessed Feb. 25, 2022).

[7] Intergovernmental Panel on Climate Change. *Climate Change 2021. The Physical Science Basis. Summary for Policymakers*. Switzerland, **2021**. Policy Report.

[8] Kheirinik, M.; Ahmed, S.; Rahmanian, N. Comparative Techno-Economic Analysis of Carbon Capture Processes: Pre-Combustion, Post-Combustion, and Oxy-Fuel Combustion Operations. *Sustainability* **2021**, *13* (24), 14. https://doi.org/10.3390/su132413567.

[9] Lackner, K. S.; Brennan, S.; Matter, J. M.; Park, A.-H. A.; Wright, A.; van der Zwaan, B. The Urgency of the Development of CO2 Capture from Ambient Air. *Proc. Natl. Acad. Sci.* **2012**, *109* (33), 13156–13162. https://doi.org/10.1073/pnas.1108765109.

[10] Metz, B.; Davidson, O.; Coninck, H. de; Loos, M.; Meyer, L. *IPCC Special Report on Carbon Dioxide Capture and Storage.*; Cambridge, United Kingdom and NewYork, USA, 2005.

[11] Madejski, P.; Chmiel, K.; Subramanian, N.; Kuś, T. Methods and Techniques for CO_2 Capture: Review of Potential Solutions and Applications in Modern Energy Technologies. *Energies* **2022**, *15*, 887. https://doi.org/10.3390/en15030887

[12] Gorny, S. M. Development of a Regenerative CO2 Air Capture Process for Sustainable Greenhouses, Instituto Superior Técnico, 2019. Master Thesis.

[13] Qian Yu. Direct Capture of CO2 from Ambient Air Using Solid Sorbents, University of Twente, 2018. PhD Thesis.

[14] Bui, M.; Adjiman, C. S.; Bardow, A.; Anthony, E. J.; Boston, A.; Brown, S.; Fennell, P. S.; Fuss, S.; Galindo, A.; Hackett, L. A.; Hallett, J. P.; Herzog, H. J.; Jackson, G.; Kemper, J.; Krevor, S.; Maitland, G. C.; Matuszewski, M.; Metcalfe, I. S.; Petit, C.; Puxty, G.; Reimer, J.; Reiner, D. M.; Rubin, E. S.; Scott, S. A.; Shah, N.; Smit, B.; Trusler, J. P. M.; Webley, P.; Wilcox, J.; Mac Dowell, N. Carbon Capture and Storage (CCS): The Way Forward. *Energy Environ. Sci.* **2018**, *11* (5), 1062–1176. https://doi.org/10.1039/C7EE02342A.

[15] Yang, M.; Ma, C.; Xu, M.; Wang, S.; Xu, L. Recent Advances in CO2 Adsorption from Air: A Review. *Curr. Pollut. Reports* **2019**, *5*, 272–293. https://doi.org/10.1007/s40726-019-00128-1

[16] Shi, X.; Xiao, H.; Azarabadi, H.; Song, J.; Wu, X.; Chen, X.; Lackner, K. S. Sorbents for the Direct Capture of CO2 from Ambient Air. *Angew. Chemie - Int. Ed.* **2020**, *59* (18), 6984–7006. https://doi.org/10.1002/anie.201906756.

[17] Breyer, C.; Fasihi, M.; Bajamundi, C.; Creutzig, F. Direct Air Capture of CO2: A Key Technology for Ambitious Climate Change Mitigation. *Joule* **2019**, *3* (9), 2053–2057. https://doi.org/10.1016/j.joule.2019.08.010.

[18] Gambhir, A.; Tavoni, M. Direct Air Carbon Capture and Sequestration: How It Works and How It Could Contribute to Climate-Change Mitigation. *One Earth* **2019**, *1* (4), 405–409. https://doi.org/10.1016/j.oneear.2019.11.006.

[19] Lackner, K.; Ziock, H.-J.; Grimes, P. Carbon Capture from Air: Is It an Option? In *24th Annual Technical Conference on Coal Utilization & Fuel Systems*; Los Alamos National Laboratory: U.S., 1999; p 12.

[20] Socolow, R.; Desmond, M.; Aines, R.; Blackstock, J.; Bolland, O.; Kaarsberg, T.; Lewis, N.; Mazzotti, M.; Pfeffer, A.; Sawyer, K.; Siirola, J.; Smit, B.; Wilcox, J. Direct Air Capture of CO2 with Chemicals. A Technology Assessment for the APS Panel on Public Affairs. *APS Phys.* **2011**, 1–119.

[21] IEA. Direct Air Capture https://www.iea.org/reports/direct-air-capture (accessed 2022 -02 -11). Scientific Report.

[22] McQueen, N.; Gomes, K. V.; McCormick, C.; Blumanthal, K.; Pisciotta, M.; Wilcox, J. A Review of Direct Air Capture (DAC): Scaling up Commercial Technologies and Innovating for the Future. *Prog. Energy* **2021**, *3* (3), 032001. https://doi.org/10.1088/2516-1083/abf1ce.

[23] Keith, D. W.; Holmes, G.; St. Angelo, D.; Heidel, K. A Process for Capturing CO2 from the Atmosphere. *Joule* **2018**, *2*, 1573–1594. https://doi.org/10.1016/j.joule.2018.05.006.

[24] Carbon Engineering. Pale Blue Dot Energy and Carbon Engineering create partnership to deploy Direct Air Capture in the UK https://carbonengineering.com/news-updates/pale-blue-dot-energy-and-carbon-engineering-partnership/ (accessed 2021 -03 -11).

[25] Ishimoto, Y.; Sugiyama, M.; Kato, E.; Moriyama, R.; Tsuzuki, K.; Kurosawa, A. Putting Costs of Direct Air Capture in Context. *SSRN Electron. J.* **2017**. https://doi.org/10.2139/ssrn.2982422.

[26] Global CCS Institute. *Global Status of CCS 2020*; 2020. Environmental Annual Report.

[27] Veneman, R. Adsorptive Systems for Post-Combustion CO2 Capture, University of Twente, 2015. PhD Thesis.

[28] Choi, S.; Drese, J. H.; Jones, C. W. Adsorbent Materials for Carbon Dioxide Capture from Large Anthropogenic Point Sources. *ChemSusChem* **2009**, *2*, 796–854. https://doi.org/10.1002/cssc.200900036.

[29] Hamdy, L. B.; Goel, C.; Rudd, J. A.; Barron, A. R.; Andreoli, E. The Application of Amine-Based Materials for Carbon Capture and Utilisation: An Overarching View. *Mater. Adv.* **2021**, *2* (18), 5843–5880. https://doi.org/10.1039/D1MA00360G.

[30] Buijs, W.; De Flart, S. Direct Air Capture of CO2 with an Amine Resin: A Molecular Modeling Study of the CO2 Capturing Process. *Ind. Eng. Chem. Res.* **2017**, *56* (43), 12297–12304. https://doi.org/10.1021/acs.iecr.7b02613.

[31] Didas, S. A.; Sakwa-Novak, M. A.; Foo, G. S.; Sievers, C.; Jones, C. W. Effect of Amine Surface Coverage on the Co-Adsorption of CO2 and Water: Spectral Deconvolution of Adsorbed Species. *J. Phys. Chem. Lett.* **2014**, *5 (23)*, 4194-4220. https://doi.org/10.1021/jz502032c.

[32] Young, J.; García-Díez, E.; Garcia, S.; van der Spek, M. The Impact of Binary Water–CO2 Isotherm Models on the Optimal Performance of Sorbent-Based Direct Air Capture Processes. *Energy Environ. Sci.* **2021**, *14*, 5377–5394. https://doi.org/10.1039/d1ee01272j.

[33] Ruthven, D. M. *Kirk-Othmer Encyclopedia of Chemical Technology*; Wiley: Hoboken, NJ, USA, 2000; Vol. 1. https://doi.org/10.1002/0471238961.

[34] Keller, J. U.; Staudt, R. *Gas Adsorption Equilibria*, 1st ed.; Kluwer Academic Publishers: Boston, 2005. https://doi.org/10.1007/b102056.

[35] UPAC. Reporting Physisorption Data for Gas/Solid Systems — with Special Reference to the Determination of Surface Area and Porosity. *Int. UNION PURE Appl. Chem.* **1984**, *81* (6), 420–430.

[36] Bos, M. J. Storage of Renewable Electricity in Methanol, University of Twente, 2019. PhD Thesis.

[37] Caplow, M. Kinetics of Carbamate Formation and Breakdown. *J. Am. Chem. Soc.* **1968**, *90* (24), 6795–6803. https://doi.org/10.1021/ja01026a041.

[38] Gabelman, A. Adsorption Basics: Part 1. *Chem. Eng. Prog.* **2017**, *113* (8), 1–6.

[39] Saha, P.; Chowdhury, S. Insight Into Adsorption Thermodynamics. *Thermodynamics* **2011**. https://doi.org/10.5772/13474.

[40] Kiełbasa, K.; Kamińska, A.; Niedoba, O.; Michalkiewicz, B. CO2 Adsorption on Activated Carbons Prepared from Molasses: A Comparison of Two and Three Parametric Models. *Materials (Basel).* **2021**, *14* (23). https://doi.org/10.3390/ma14237458.

[41] Do, D. D. *Adsorption Analysis: Equilibria and Kinetics*; Series on Chemical Engineering; Imperial College Press: London, 1998; Vol. 2. https://doi.org/10.1142/p111.

[42] Flaig, R. W.; Osborn Popp, T. M.; Fracaroli, A. M.; Kapustin, E. A.; Kalmutzki, M. J.; Altamimi, R. M.; Fathieh, F.; Reimer, J. A.; Yaghi, O. M. The Chemistry of CO2 Capture in an Amine-Functionalized Metal-Organic Framework under Dry and Humid Conditions. *J. Am. Chem. Soc.* **2017**, *139*, 12125–12128. https://doi.org/10.1021/jacs.7b06382.

[43] García Martínez, J. B. Study of Water Adsorption on an Amine Adsorbent for Direct Air Capture of CO2, University of Twente, 2020. Master Thesis.

[44] Quirijns, E. J.; Van Boxtel, A. J. B.; Van Loon, W. K. P.; Van Straten, G. Sorption Isotherms, GAB Parameters and Isosteric Heat of Sorption. *J. Sci. Food Agric.* **2005**, *85* (11), 1805–1814. https://doi.org/10.1002/jsfa.2140.

[45] Stampi-Bombelli, V.; van der Spek, M.; Mazzotti, M. Analysis of Direct Capture of CO2 from Ambient Air via Steam-Assisted Temperature–Vacuum Swing Adsorption. *Adsorption* **2020**, *26* (7), 1183–1197. https://doi.org/10.1007/s10450-020-00249-w.

[46] Yu, Q.; Delgado, J. D. L. P.; Veneman, R.; Brilman, D. W. F. Stability of a Benzyl Amine Based CO2 Capture Adsorbent in View of Regeneration Strategies. *Ind. Eng. Chem. Res.* **2017**, *56* (12), 3259–3269. https://doi.org/10.1021/acs.iecr.6b04645.

[47] Sanz-Pérez, E. S.; Murdock, C. R.; Didas, S. A.; Jones, C. W. Direct Capture of CO2 from Ambient Air. *Chem. Rev.* **2016**, *116* (19), 11840–11876. https://doi.org/10.1021/acs.chemrev.6b00173.

[48] Shi, X., Xiao, H., Azarabadi, H., Song, J., Wu, X., Chen, X., Lackner, K. Sorbents for the Direct Capture of CO2 from Ambient Air. *Angewandte Chemie - International Edition* **2020**, 59 (18), 6984–7006. https://doi.org/10.1002/anie.201906756.

[49] Gelles, T.; Lawson, S.; Rownaghi, A. A.; Rezaei, F. Recent Advances in Development of Amine Functionalized Adsorbents for CO2 Capture. *Adsorption* **2020**, *26* (1), 5–50. https://doi.org/10.1007/s10450-019-00151-0.

[50] Didas, S. A. Structural Properties of Aminosilica Materials for CO2 Capture, Georgia Institute of Technology, 2014. PhD Thesis.

[51] Lanxess. LEWATIT® VP OC 1065 https://lanxess.com/en/Products-and-Solutions/Products/1/LEWATIT--VP-OC-1065 (accessed 2021 -10 -10).

[52] Alesi, W. R.; Kitchin, J. R. Evaluation of a Primary Amine-Functionalized Ion-Exchange Resin for CO2 Capture. *Ind. Eng. Chem. Res.* **2012**, *51* (19), 6907–6915. https://doi.org/10.1021/ie300452c.

[53] Veneman, R.; Zhao, W.; Li, Z.; Cai, N.; Brilman, D. W. F. Adsorption of CO2 and H2o on Supported Amine Sorbents. *Energy Procedia* **2014**, *63*, 2336–2345. https://doi.org/10.1016/j.egypro.2014.11.254.

[54] Alesi, W. R.; Kitchin, J. R. Evaluation of a Primary Amine-Functionalized Ion-Exchange Resin for CO 2 Capture. *Ind. Eng. Chem. Res.* **2012**, *51* (19), 6907–6915. https://doi.org/10.1021/ie300452c.

[55] Frigka, N. Experimental Study of CO2 and H2O Adsorption, University of Twente, 2020. Master Thesis.

[56] Arstad, B.; Blom, R.; Swang, O. CO2 Absorption in Aqueous Solutions of Alkanolamines: Mechanistic Insight from Quantum Chemical Calculations. *J. Phys. Chem. A* **2007**, *111* (7), 1222–1228. https://doi.org/10.1021/jp065301v.

[57] Bacsik, Z.; Ahlsten, N.; Ziadi, A.; Zhao, G.; Garcia-Bennett, A. E.; Martín-Matute, B.; Hedin, N. Mechanisms and Kinetics for Sorption of CO2 on Bicontinuous Mesoporous Silica Modified with N-Propylamine. *Langmuir* **2011**, *27* (17), 11118–11128. https://doi.org/10.1021/la202033p.

[58] Danon, A.; Stair, P. C.; Weitz, E. FTIR Study of CO 2 Adsorption on Amine-Grafted SBA-15: Elucidation of Adsorbed Species. *J. Phys. Chem. C* **2011**, *115* (23), 11540–11549. https://doi.org/10.1021/jp200914v.

[59] Smal, I. M.; Yu, Q.; Veneman, R.; Fränzel-Luiten, B.; Brilman, D. W. F. TG-FTIR Measurement of CO2-H2O Co-Adsorption for CO2 Air Capture Sorbent Screening. *Energy Procedia* **2014**, *63*, 6834–6841. https://doi.org/10.1016/j.egypro.2014.11.717.

[60] Elfving, J.; Bajamundi, C.; Kauppinen, J. Characterization and Performance of Direct Air Capture Sorbent. *Energy Procedia* **2017**, *114*, 6087–6101. https://doi.org/10.1016/j.egypro.2017.03.1746.

[61] Wang, Y.; Jia, H.; Fang, X.; Qiu, Z.; Du, T. CO2 and Water Vapor Adsorption Properties of Framework Hybrid W-ZSM-5/Silicalite-1 Prepared from RHA. *RSC Adv.* **2020**, *10* (41), 24642–24652. https://doi.org/10.1039/d0ra03736b.

[62] Kortunov, P. V.; Siskin, M.; Paccagnini, M.; Thomann, H. CO2 Reaction Mechanisms with Hindered Alkanolamines: Control and Promotion of Reaction Pathways. *Energy and Fuels* **2016**, *30* (2), 1223–1236. https://doi.org/10.1021/acs.energyfuels.5b02582.

[63] Mafra, L.; Čendak, T.; Schneider, S.; Wiper, P. V.; Pires, J.; Gomes, J. R. B.; Pinto, M. L. Structure of Chemisorbed CO 2 Species in Amine-Functionalized Mesoporous Silicas Studied by Solid-State NMR and Computer Modeling. *J. Am. Chem. Soc.* **2017**, *139* (1), 389–408. https://doi.org/10.1021/jacs.6b11081.

[64] Afonso, R.; Sardo, M.; Mafra, L.; Gomes, J. R. B. Unravelling the Structure of Chemisorbed CO2 Species in Mesoporous Aminosilicas: A Critical Survey. *Environ. Sci. Technol.* **2019**, *53* (5), 2758–2767. https://doi.org/10.1021/acs.est.8b05978.

[65] Pinto, M. L.; Mafra, L.; Guil, J. M.; Pires, J.; Rocha, J. Adsorption and Activation of CO2 by Amine-Modified Nanoporous Materials Studied by Solid-State NMR and 13CO2 Adsorption. *Chem. Mater.* **2011**, *23* (6), 1387–1395. https://doi.org/10.1021/cm1029563.

[66] Lee, K. H.; Kim, S. J.; Park, H. S.; Lim, B. W.; Lee, B.; Park, Y. J.; Nam, W.; Hur, N. H. Stable Carbamate Pathway towards Organic–Inorganic Hybrid Perovskites and Aromatic Imines. *RSC Adv.* **2020**, *10* (62), 38055–38062. https://doi.org/10.1039/D0RA07814J.

[67] Čendak, T.; Sequeira, L.; Sardo, M.; Valente, A.; Pinto, M. L.; Mafra, L. Detecting Proton Transfer in CO2 Species Chemisorbed on Amine-Modified Mesoporous Silicas by Using 13C NMR Chemical Shift Anisotropy and Smart Control of Amine Surface Density. *Chem. - A Eur. J.* **2018**, *24* (40), 10136–10145. https://doi.org/10.1002/chem.201800930.

[68] P. V. Danckwerts, "The reaction of CO2 with ethanolamines," *Chem Eng Sci*, vol. 34, no. 4, pp. 443–446, 1979, doi: 10.1016/0009-2509(79)85087-3.

[69] Kortunov, P. V.; Siskin, M.; Baugh, L. S.; Calabro, D. C. In Situ Nuclear Magnetic Resonance Mechanistic Studies of Carbon Dioxide Reactions with Liquid Amines in Non-Aqueous Systems: Evidence for the Formation of Carbamic Acids and Zwitterionic Species. *Energy and Fuels* **2015**, *29* (9), 5940–5966. https://doi.org/10.1021/acs.energyfuels.5b00985.

[70] Hahn, M. W.; Steib, M.; Jentys, A.; Lercher, J. A. Mechanism and Kinetics of CO2 Adsorption on Surface Bonded Amines. *J. Phys. Chem. C* **2015**, *119* (8), 4126–4135. https://doi.org/10.1021/jp512001t.

[71] Kortunov, P.; Baugh, L.; Calabro, D.; Siskin, M. High CO2 To Amine Adsorption Capacity Scrubbing Processes. Patent WO2012034027A1, 2012.

[72] Li, K.; Kress, J. D.; Mebane, D. S. The Mechanism of CO2 Adsorption under Dry and Humid Conditions in Mesoporous Silica-Supported Amine Sorbents. *J. Phys. Chem. C* **2016**, *120* (41), 23683–23691. https://doi.org/10.1021/acs.jpcc.6b08808.

[73] Didas, S. A.; Zhu, R.; Brunelli, N. A.; Sholl, D. S.; Jones, C. W. Thermal, Oxidative and CO2 Induced Degradation of Primary Amines Used for CO2 Capture: Effect of Alkyl Linker on Stability. *J. Phys. Chem. C* **2014**, *118* (23), 12302–12311. https://doi.org/10.1021/jp5025137.

[74] Said, R. Ben; Kolle, J. M.; Essalah, K.; Tangour, B.; Sayari, A. A Unified Approach to CO2-Amine Reaction Mechanisms. *ACS Omega* **2020**, *5* (40), 26125–26133. https://doi.org/10.1021/acsomega.0c03727.

[75] Yu, J.; Chuang, S. S. C. The Structure of Adsorbed Species on Immobilized Amines in CO2 Capture: An in Situ IR Study. *Energy and Fuels* **2016**, *30* (9), 7579–7587. https://doi.org/10.1021/acs.energyfuels.6b01423.

[76] Y. Zhai and S. S. C. Chuang, "The Nature of Adsorbed Carbon Dioxide on Immobilized Amines during Carbon Dioxide Capture from Air and Simulated Flue Gas," *Energy Technology*, vol. 5, no. 3, pp. 510–519, 2017, doi: 10.1002/ente.201600685.

[77] Züttel, A. Materials for Hydrogen Storage. *Mater. Today* **2003**, *6* (9), 24–33. https://doi.org/10.1016/S1369-7021(03)00922-2.

[78] Sardo, M.; Afonso, R.; Juźków, J.; Pacheco, M.; Bordonhos, M.; Pinto, M. L.; Gomes, J. R. B.; Mafra, L. Unravelling Moisture-Induced CO 2 Chemisorption Mechanisms in Amine-Modified Sorbents at the Molecular Scale. *J. Mater. Chem. A* **2021**, *9* (9), 5542–5555. https://doi.org/10.1039/D0TA09808F.

[79] Yu, J.; Zhai, Y.; Chuang, S. S. C. Water Enhancement in CO2 Capture by Amines: An Insight into CO2-H2O Interactions on Amine Films and Sorbents. *Ind. Eng. Chem. Res.* **2018**, *57* (11), 4052–4062. https://doi.org/10.1021/acs.iecr.7b05114.

[80] Gebald, C.; Wurzbacher, J.; Borgschulte, A.; Zimmermann, T.; Steinfeld, A. Single-Component and Binary CO2 and H2O Adsorption of Amine- Functionalized Cellulose. *Environ. Sci. Technol.* **2014**, 2497−2504.

[81] Young, J.; García-Díez, E.; Garcia, S.; Ireland, C.; Smit, B.; van der Spek, M. Investigating H2O and CO2 Co-Adsorption on Amine-Functionalised Solid Sorbents for Direct Air Capture. *SSRN Electron. J.* **2021**, No. March, 1–7. https://doi.org/10.2139/ssrn.3814942.

[82] Liu, Q.; Xiong, B.; Shi, J.; Tao, M.; He, Y.; Shi, Y. Enhanced Tolerance to Flue Gas Contaminants on Carbon Dioxide Capture Using Amine-Functionalized Multiwalled Carbon Nanotubes. *Energy and Fuels* **2014**, *28* (10), 6494–6501. https://doi.org/10.1021/ef501614m.

[83] Lee, A. S.; Kitchin, J. R. Chemical and Molecular Descriptors for the Reactivity of Amines with CO2. *Ind. Eng. Chem. Res.* **2012**, *51* (42), 13609–13618. https://doi.org/10.1021/ie301419q.

[84] Chen, C. H.; Shimon, D.; Lee, J. J.; Mentink-Vigier, F.; Hung, I.; Sievers, C.; Jones, C. W.; Hayes, S. E. The "Missing" Bicarbonate in CO2 Chemisorption Reactions on Solid Amine Sorbents. *J. Am. Chem. Soc.* **2018**, *140* (28), 8648–8651. https://doi.org/10.1021/jacs.8b04520.

[85] Aziz, B.; Hedin, N.; Bacsik, Z. Quantification of Chemisorption and Physisorption of Carbon Dioxide on Porous Silica Modified by Propylamines: Effect of Amine Density. *Microporous Mesoporous Mater.* **2012**, *159*, 42–49. https://doi.org/10.1016/j.micromeso.2012.04.007.

[86] Yu, J.; Chuang, S. S. C. The Role of Water in CO2 Capture by Amine. *Ind. Eng. Chem. Res.* **2017**, *56* (21), 6337–6347. https://doi.org/10.1021/acs.iecr.7b00715.

[87] Vries, M. De. Enhanced Carbon Dioxide Adsorption from Air by Using Water, University of Twente, 2020. Bachelor Thesis.

[88] Buck, A. L. New Equations for Computing Vapor Pressure and Enhancement Factor. *J. Appl. Meteorol.* **1981**, *20* (12), 1527-1532.

[89] Schellevis, M.; van Schagen, T.; Brilman, W. Process Optimization of a Fixed Bed Reactor System for Direct Air Capture. *SSRN Electron. J.* **2021**, No. March. https://doi.org/10.2139/ssrn.3821508.

[90] MathWorks®. Evaluating Goodness of Fit. https://www.mathworks.com/help/curvefit/evaluating-goodness-of-fit.html (accessed 2022 -03 -03).

[91] KnowledgeHut. How to Interpret R Squared and Goodness of Fit in Regression Analysis. https://www.knowledgehut.com/blog/data-science/interpret-r-squared-and-goodness-fit-regression-analysis (accessed 2022 -04 -15).

[92] Frost, J. How To Interpret R-squared in Regression Analysis. https://statisticsbyjim.com/regression/interpret-r-squared-regression/ (accessed 2022 -04 -17).

[93] Chen, Q.; Tian, Y.; Li, P.; Yan, C.; Pang, Y.; Zheng, L.; Deng, H.; Zhou, W.; Meng, X. Study on Shale Adsorption Equation Based on Monolayer Adsorption, Multilayer Adsorption, and Capillary Condensation. *J. Chem.* **2017**, *2017*. https://doi.org/10.1155/2017/1496463.

A

EQUILIBRIUM ISOTHERMS

A.1 Langmuir Isotherm

The Langmuir model (Equation A.1) is a simple, theoretical isotherm model that can describe well systems with weakly adsorbed gases. Some of its assumptions include the adsorbent surface being homogeneous and flat (considered ideal), the formation of a single layer, and no interactions between adsorbed molecules [38]. This expression is adequate for a type I isotherm given that at low partial pressures, the fraction adsorbed varies linearly with partial pressure, known as the first-order region or the Henry's law region [39]. However, the number of available sites decreases as the pressure increases, and further adsorption becomes increasingly limited. At some point, the amount adsorbed stagnates, and the isotherm reaches a plateau, denominated as a zero-order region [38].

$$q_e = \frac{q_s b P_{CO2}}{1 + (b P_{CO2})} \tag{A. 1}$$

A.2 BET Isotherm

The Brunauer-Emmet-Teller (BET) model was created as an extension of the Langmuir isotherm (see equation A.2) to account for monolayer and multilayer formation. It assumes that the interaction between adsorbate and adsorbent surface is much larger than that between neighboring molecules [93]. The model is appropriate for porous materials and is frequently applied to calculate the specific surface area of porous media [35].

$$q_e = q_m \frac{C \, {p_{H2O}}/{P_{H2O}^{sat}}}{\left(1 - {p_{H2O}}/{P_{H2O}^{sat}}\right)\left(1 + (C-1) \, {p_{H2O}}/{P_{H2O}^{sat}}\right)} \quad \text{(A. 2)}$$

Where parameter C is the BET constant describing the adsorbent–adsorbate interaction intensity [—]. Although parameter C is referred to as the difference of free energy between the monolayer and multilayers, it does not provide a quantitative measure of enthalpy of adsorption. It merely indicates the magnitude of the adsorbent-adsorbate interaction energy [93].

B

LEWATIT VP OC 1065

B.1 Specifications

Lewatit is a commercial amine-functionalized Anion Exchange Resin (AER) meso-porous adsorbent. Structurally, it is a benzylamine cross-linked polymer based on a polystyrene (PS) and divinyl benzene (DVB) backbone. Its properties are shown in Table B.1.

Table B.1 - Physical and chemical properties of Lewatit VP OC 1065.

Parameter	**Unit**		**Reference**
Functional group	-	primary amine	[51]
Matrix	-	crosslinked polystyrene	[51]
Appearance	-	opaque beads	[51]
Water retention	wt. %	[65, 70]	[51]
BET Surface area	$m^2.g^{-1}$	50	[51]
Pore volume	$cm^3.g^{-1}$	0.27	[51]
Pore diameter	nm	25	[51]
Stability	ºC	[-20, 100]	[51]
Maximum Storability	years	2	[51]

C

PARAMETERS FROM LITERATURE

The fitting procedure was based in the implementation of experimental data from single adsorption and co-adsorption into theoretical model fits. Results from CO_2 and H_2O adsorption were described the Tóth and GAB models, respectively, as shown in Table C.1 and C.2. Fitted values found in literature are presented too. The co-adsorption behavior and experimental values (i.e., CO_2 in presence of moisture) is fitted into three models: Mechanistic, WADST and Stampi-Bombelli, as presented in Tables C.3, C.4 and C.4.

C.1 Tóth Model

Table C.1 - Fitted parameters from literature for the Tóth adsorption equilibrium model.

Tóth Model			
Parameter	Veneman *et al.* [27]	M.Bos [36]	Units
q_{s0}	3.40	3.40	$mol.kg^{-1}$
χ	0	0	-
T_0	353.15	353.15	K^{-1}
b_0	408.84	93.0	bar^{-1}
ΔH_{ads}	86.7	95.3	$kJ.mol^{-1}$
t_0	0.30	0.37	-
α	0.14	0.33	-
NSD	15.4	7.7	%

C.2 GAB Model

Table C.2 - Fitted parameters from literature for the GAB adsorption equilibrium model.

GAB Model		
Parameter	J. G. Martínez [43]	Units
ΔH_c	12.2	kJ.mol^{-1}
ΔH_K	5.9	kJ.mol^{-1}
C_0	1.72E-02	-
k_0	7.14E-02	-
q_m	3.10	mol.kg^{-1}
NSD	15.8	%

C.3 Co-Adsorption Models

Table C.3 - Fitted parameters from literature for the Mechanistic co-adsorption equilibrium model.

Mechanistic Model		
Parameter	Young *et al.* [32]	Units
A	1.535	mol.kg^{-1}
ϕ_{dry}	1	-
$f_{blocked}$	0.433	-
k	0.795	-
n	1.425	-
ΔH_r	130155	J.mol^{-1}

Table C.4 - Fitted parameters from literature for the WADST co-adsorption equilibrium model.

WADST Model		
Parameter	Young *et al.* [32]	Units
$q_{s0,wet}$	9.035	mol.kg^{-1}
χ_{wet}	0	-
$b_{0,wet}$	1.23E-18	Pa^{-1}
$\Delta H_{ads,wet}$	203687	J.mol^{-1}
$t_{0,wet}$	0.053	-
$\alpha_{,\,wet}$	0.053	-
A	1.532	mol.kg^{-1}

Table C.5 - Fitted parameters from literature for the Stampi-Bombelli co-adsorption equilibrium model.

Stampi-Bombelli Model			
Parameter	Stampi *et al.* [45]	Young *et al.* [32]	Units
β	28.907	5.612	-
γ	0.006	-0.137	-

D

PLOTS FROM MODEL FITTING

D.1 Co-Adsorption Models

In this Appendix all the plots resultant from data fitting are presented for the three models from literature (i.e., WADST model, Mechanistic model and Stampi-Bombelli Model), as well as the empirical model proposed in this study. The adsorption capacity is plotted against relative humidity, with RH of 0% - 90% at temperatures 5 – 35 °C, and partial pressures of 40, 200, and 1000 Pa. As referred in Chapter 4, the application of the experimental values showed both good and poor agreements depending on the conditions. Experimental trends were well characterized for lower concentrations of CO_2 (~400 ppm), found in ambient air. These trends are represented in Figures D.1, D.2 and D.3. As CO_2 concentrations increase, some disagreements between the model fitting and experimental results are visible. Figures D.4, D.5 and D.5, at P_{CO2}= 200 Pa, present better fittings at moderate temperatures (i.e., T=15ºC and T=25ºC) than extremely low or high conditions, as discussed in Chapter 4.3.2. At P_{CO2}=1000 Pa, for Figures D.7, D.8 and D.9, no model is able of describing the obtained data.

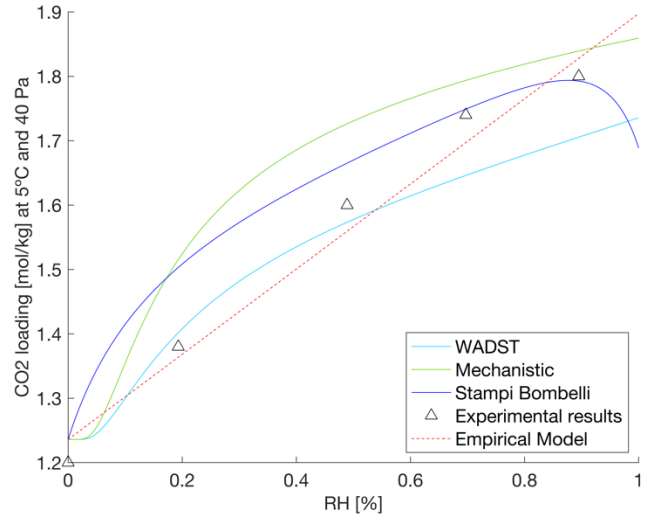

Figure D.1 - Fitting representation of the adsorption capacity plotted against relative humidity (RH), from the three models found in literature and the proposed empirical model. The conditions are at 5°C and 40 Pa.

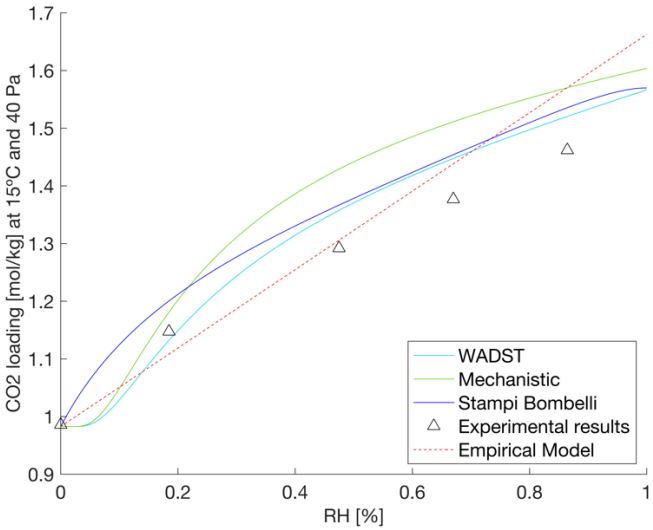

Figure D.2 - Fitting representation of the adsorption capacity plotted against relative humidity (RH), from the three models found in literature and the proposed empirical model. The conditions are at 15°C and 40 Pa.

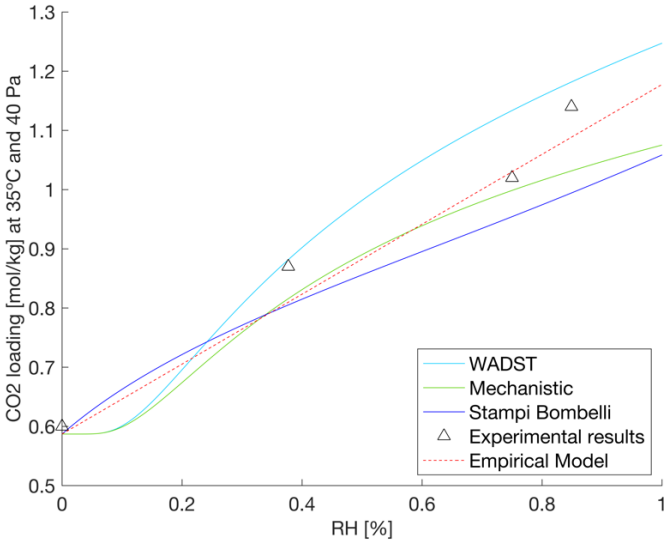

Figure D.3 - Fitting representation of the adsorption capacity plotted against relative humidity (RH), from the three models found in literature and the proposed empirical model. The conditions are at 35ºC and 40 Pa.

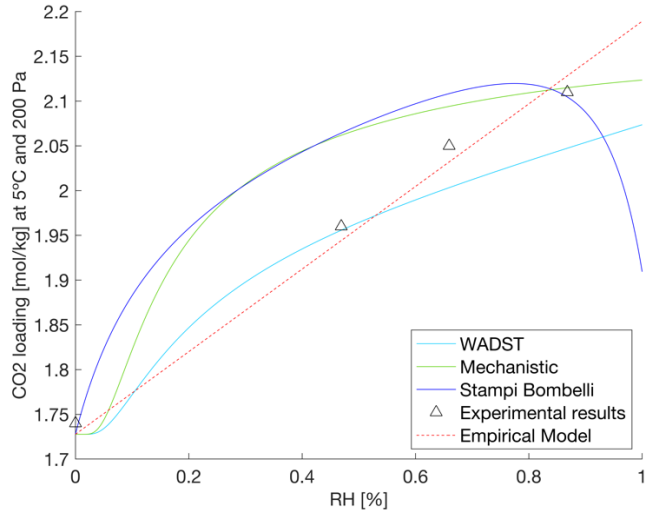

Figure D.4 - Fitting representation of the adsorption capacity plotted against relative humidity (RH), from the three models found in literature and the proposed empirical model. The conditions plots are at 5ºC and 200 Pa.

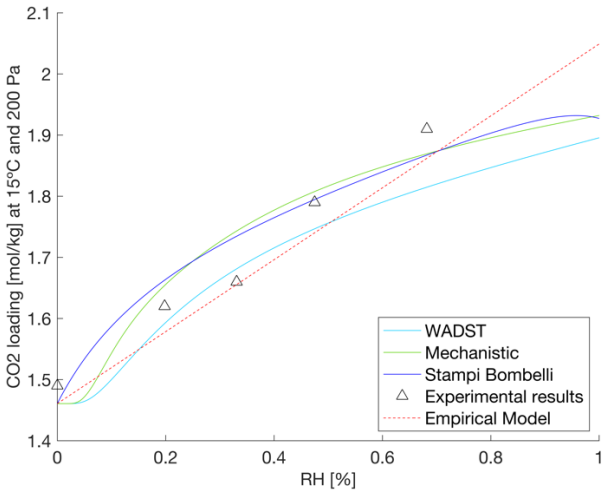

Figure D.5 - Fitting representation of the adsorption capacity plotted against relative humidity (RH), from the three models found in literature and the proposed empirical model. The conditions plots are at 15ºC and 200 Pa.

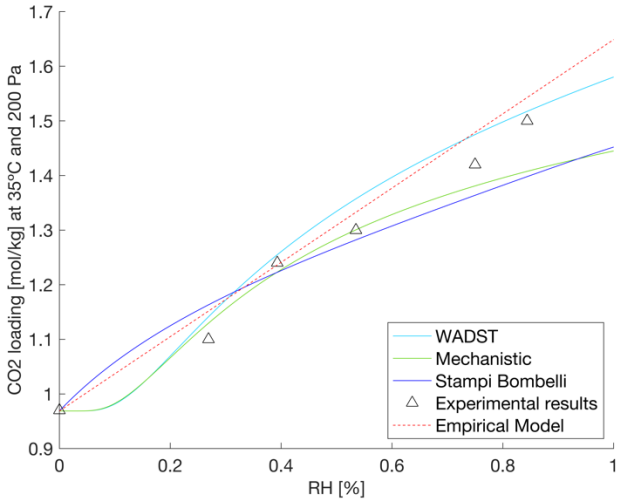

Figure D.6 - Fitting representation of the adsorption capacity plotted against relative humidity (RH), from the three models found in literature and the proposed empirical model. The conditions are at 35ºC and 200 Pa.

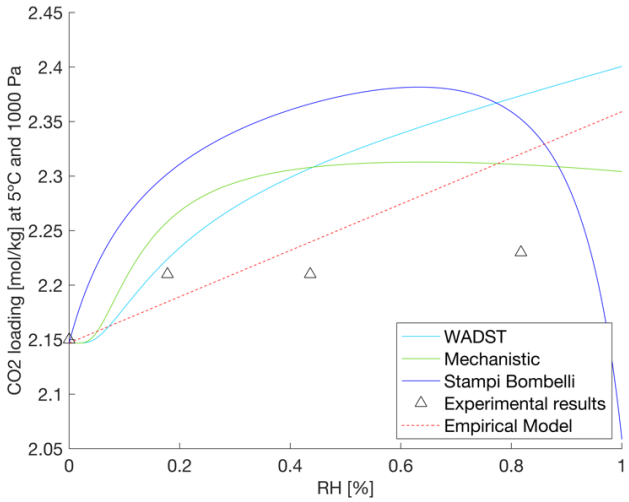

Figure D.7 - Fitting representation of the adsorption capacity plotted against relative humidity (RH), from the three models found in literature and the proposed empirical model. The conditions are at 5°C and 1000 Pa.

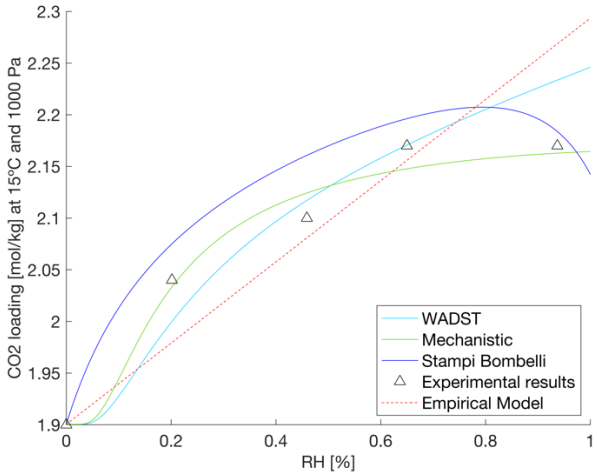

Figure D.8 - Fitting representation of the adsorption capacity plotted against relative humidity (RH), from the three models found in literature and the proposed empirical model. The conditions are at 15°C and 1000 Pa.

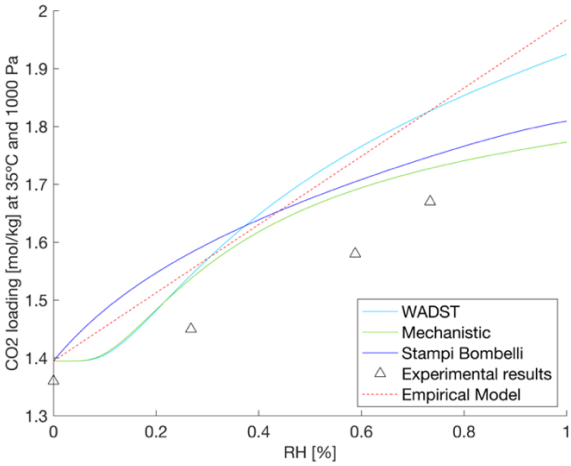

Figure D.9 - Fitting representation of the adsorption capacity plotted against relative humidity (RH), from the three models found in literature and the proposed empirical model. The conditions are at 35°C and 1000 Pa.

2022

SARA RODRIGUES AMORIM

WATER ENHANCEMENT ON CO_2 ADSORPTION: EQUILIBRIUM STUDIES ON AN AMINE SORBENT FOR DIRECT AIR CAPTURE

NOVA SCHOOL OF SCIENCE & TECHNOLOGY